



**HAL**  
open science

## Experimental study of arsenic speciation in vapor phase to 500°C: Implications for As transport and fractionation in low-density crustal fluids and volcanic gases.

Gleb S. Pokrovski, Ildar V. Zakirov, Jacques Roux, Denis Testemale,  
Jean-Louis Hazemann, Andrew Y. U. Bychkov, Galina V. Golikova

### ► To cite this version:

Gleb S. Pokrovski, Ildar V. Zakirov, Jacques Roux, Denis Testemale, Jean-Louis Hazemann, et al.. Experimental study of arsenic speciation in vapor phase to 500°C: Implications for As transport and fractionation in low-density crustal fluids and volcanic gases.. *Geochimica et Cosmochimica Acta*, 2002, 66, pp.(19) 3453-3480. 10.1016/S0016-7037(02)00946-8 . hal-00077601

**HAL Id: hal-00077601**

**<https://insu.hal.science/hal-00077601>**

Submitted on 24 Jan 2013

**HAL** is a multi-disciplinary open access archive for the deposit and dissemination of scientific research documents, whether they are published or not. The documents may come from teaching and research institutions in France or abroad, or from public or private research centers.

L'archive ouverte pluridisciplinaire **HAL**, est destinée au dépôt et à la diffusion de documents scientifiques de niveau recherche, publiés ou non, émanant des établissements d'enseignement et de recherche français ou étrangers, des laboratoires publics ou privés.



PII S0016-7037(02)00946-8

## Experimental study of arsenic speciation in vapor phase to 500°C: Implications for As transport and fractionation in low-density crustal fluids and volcanic gases

GLEB S. POKROVSKI,<sup>1,\*</sup> ILДАР V. ZAKIROV,<sup>2</sup> JACQUES ROUX,<sup>1</sup> DENIS TESTEMALE,<sup>3</sup> JEAN-LOUIS HAZEMANN,<sup>3</sup> ANDREW YU. BYCHKOV,<sup>4</sup> and GALINA V. GOLIKOVA<sup>4</sup><sup>1</sup>Institut des Sciences de la Terre d'Orléans (ISTO), UMR 6133 of CNRS, 1A rue de la F erollerie, 45071 Orl ans cedex 2, France<sup>2</sup>Institute of Experimental Mineralogy (IEM-RAS), Chernogolovka, Russia<sup>3</sup>Laboratoire de Cristallographie, UPR 5031 of CNRS, B.P. 166, 38042 Grenoble09, France<sup>4</sup>Geological Department, Moscow State University, Moscow, Russia

(Received December 3, 2001; accepted in revised form April 22, 2002)

**Abstract**—The stoichiometry and stability of arsenic gaseous complexes were determined in the system As–H<sub>2</sub>O ± NaCl ± HCl ± H<sub>2</sub>S at temperatures up to 500°C and pressures up to 600 bar, from both measurements of As<sup>(III)</sup> and As<sup>(V)</sup> vapor–liquid and vapor–solid partitioning, and X-ray absorption fine structure (XAFS) spectroscopic study of As<sup>(III)</sup>-bearing aqueous fluids. Vapor–aqueous solution partitioning for As<sup>(III)</sup> was measured from 250 to 450°C at the saturated vapor pressure of the system (P<sub>sat</sub>) with a special titanium reactor that allows in situ sampling of the vapor phase. The values of partition coefficients for arsenious acid (H<sub>3</sub>AsO<sub>3</sub>) between an aqueous solution (pure H<sub>2</sub>O) and its saturated vapor (K = mAs<sub>vapor</sub>/mAs<sub>liquid</sub>) were found to be independent of As<sup>(III)</sup> solution concentrations (up to ~1 to 2 mol As/kg) and equal to 0.012 ± 0.003, 0.063 ± 0.023, and 0.145 ± 0.020 at 250, 300, and 350°C, respectively. These results are interpreted by the formation, in the vapor phase, of As(OH)<sub>3</sub>(gas), similar to the aqueous As hydroxide complex dominant in the liquid phase. Arsenic chloride or sulfide gaseous complexes were found to be negligible in the presence of HCl or H<sub>2</sub>S (up to ~0.5 mol/kg of vapor). XAFS spectroscopic measurements carried out on As<sup>(III)</sup>-H<sub>2</sub>O (±NaCl) solutions up to 500°C demonstrate that the As(OH)<sub>3</sub> complex dominates As speciation both in dense H<sub>2</sub>O–NaCl fluids and low-density supercritical vapor. Vapor–liquid partition coefficients for As<sup>(III)</sup> measured in the H<sub>2</sub>O–NaCl system up to 450°C are consistent with the As speciation derived from these spectroscopic measurements and can be described by a simple relationship as a function of the vapor-to-liquid density ratio and temperature. Arsenic<sup>(III)</sup> partitioning between vapor and As-concentrated solutions (>2 mol As/kg) or As<sub>2</sub>O<sub>3</sub> solid is consistent with the formation, in the vapor phase, of both As<sub>4</sub>O<sub>6</sub> and As(OH)<sub>3</sub>. Arsenic<sup>(V)</sup> (arsenic acid, H<sub>3</sub>AsO<sub>4</sub>) vapor–liquid partitioning at 350°C for dilute aqueous solution was interpreted by the formation of AsO(OH)<sub>3</sub> in the vapor phase.

The results obtained were combined with the corresponding properties for the aqueous As(III) hydroxide species to generate As(OH)<sub>3</sub>(gas) thermodynamic parameters. Equilibrium calculations carried out by using these data indicate that As(OH)<sub>3</sub>(gas) is by far the most dominant As complex in both volcanic gases and boiling hydrothermal systems. This species is likely to be responsible for the preferential partition of arsenic into the vapor phase as observed in fluid inclusions from high-temperature (400 to 700°C) Au–Cu (–Sn, –W) magmatic-hydrothermal ore deposits. The results of this study imply that hydrolysis and hydration could be also important for other metals and metalloids in the H<sub>2</sub>O–vapor phase. These processes should be taken into account to accurately model element fractionation and chemical equilibria during magma degassing and fluid boiling. Copyright © 2002 Elsevier Science Ltd

### 1. INTRODUCTION

The great majority of natural processes in the Earth's crust occur in the presence of fluid phases, aqueous or gaseous. Until recently, a huge number of experimental, theoretical, and field studies have been devoted to the transport of metals and the formation of ore deposits by dense aqueous fluids. However, fewer experimental and geological information is available on metal behavior and transport in low-density vapors that are ubiquitous in hydrothermal and volcanic environments. Arsenic, one of the most common components in such environments, is often present in significant amounts in minerals, fluid, and gas phases throughout different stages of the crustal fluid evolution, like the separation of hot volatile-rich magmatic fluids from a crystallizing deep pluton, the vapor–brine segre-

gation and boiling of the ascending fluids in porphyry-style and epithermal ore deposits, and the fumarolic activity in modern volcanic areas (Goldschmidt, 1954; Heinrich and Eadington, 1986; Ballantine and Moore, 1988; Migdisov and Bychkov, 1998). Knowledge about the chemical status and solubility of arsenic in the vapor phase is necessary to account for its distribution during the magmatic-to-hydrothermal/volcanic evolution of As-bearing fluids and to better understand the relative importance of different processes (boiling, fluid mixing, fluid–host rock interactions) leading to the ore precipitation of arsenic and related metals. The aim of this article is to provide new data on the identity and stability of As species existing in water vapor and to apply these results to better understand the role of the vapor phase in As transport and fractionation.

The important role of the high-temperature vapors in the geochemistry of this relatively volatile element has long been

\* Author to whom correspondence should be addressed (gleb@cnsr-orleans.fr).

recognized from analyses of volcanic gas condensates and sublimates. Arsenic concentrations often attain 1 to 10 ppm in the vapor condensates of volcanic gases sampled at temperatures from 400 to 900°C (e.g., Symonds, 1990; Mambo et al., 1991), and up to 0.1 wt% in mineral sublimates and incrustations precipitated from the gaseous phase during volcanic eruptions (e.g., Symonds et al., 1987; Quisefit et al., 1989). This corresponds to As enrichment factors in the gas phase with respect to the magma of 100 to 1000, suggesting an important transfer of As into the hydrosphere and atmosphere during magma degassing and volcanic eruptions. At lower temperatures (<350°C), in water-dominated active hydrothermal systems, As was found to preferentially concentrate into the liquid aqueous phase. Arsenic vapor–liquid fractionation factors, measured in hot springs of modern geothermal fields, typically range from 0.001 to 0.01 at temperatures of 150 to 300°C (Smith et al., 1987; Ballantine and Moore, 1988; and references therein). Recent measurements of element concentrations in coexisting high-density brine (H<sub>2</sub>O–NaCl) and low-density vapor (H<sub>2</sub>O–H<sub>2</sub>S–HCl) inclusions in quartz from magmatic-hydrothermal Cu–Au–Sn–Mo–W–As deposits, formed at temperatures from 400 to 700°C, have demonstrated strong enrichments of As, B, Cu, and Au in the vapor phase, in contrast to other metals (e.g., Fe, W, Pb, Zn, Sb) that preferentially concentrate in the liquid NaCl-rich phase (Audétat et al., 1998, Audétat et al., 2000; Heinrich et al., 1999; Ulrich et al., 1999). Arsenic vapor/liquid partition coefficients derived in these studies range from 1 to 10 at temperatures from 450 to 650°C and pressures corresponding to the two-phase equilibrium in the H<sub>2</sub>O–NaCl system (300 to 500 bar). Vapor separation thus allows selective transport of As and associated metals (Au, Cu), and can greatly affect the evolution and distribution of magmatic-hydrothermal ore deposits (Heinrich et al., 1999). Quantitative understanding of As transport in the low-density fluid phase is, however, hampered by the lack of data on As chemical species identity and stability in this phase.

In recent years, effort has been made toward acquisition of thermodynamic and structural data for As aqueous species existing in high-temperature dense aqueous solution (density  $\geq 0.4 \text{ g cm}^{-3}$ ) via both solubility measurements of As-bearing minerals and spectroscopic techniques. These studies have shown that As(III) hydroxide (mainly As(OH)<sub>3</sub>) and, to a lesser extent, sulfide (H<sub>0–3</sub>As<sub>1–3</sub>S<sub>3–6</sub>) aqueous species are the main As complexes in natural hydrothermal solutions depending on temperature, pH, and H<sub>2</sub>S content (Akinfiev et al., 1992; Helz et al., 1995; Pokrovski et al., 1996, 2002a, and references therein). These and other earlier studies allowed generation of a consistent set of thermodynamic properties in the system H<sub>2</sub>O–As<sub>2</sub>O<sub>3</sub>–As<sub>2</sub>S<sub>3</sub>–FeAsS and thus permitted better constraint of the stabilities and solubilities of the main As minerals such as arsenolite, orpiment, realgar, and arsenopyrite at hydrothermal conditions (Akinfiev et al., 1992; Pokrovski et al., 1996, Pokrovski et al., 2002a). However, much less is known about arsenic speciation in low-density supercritical fluids (density  $\leq \sim 0.3 \text{ g cm}^{-3}$ ), hydrothermal steams, and volcanic gases. Currently available databases (e.g., Pankratz, 1982; Gurvich et al., 1993; Symonds and Reed, 1993) present only thermodynamic properties of anhydrous gaseous species of arsenic (e.g., As<sub>4</sub>, As<sub>4</sub>O<sub>6</sub>, AsO, AsS, AsCl<sub>3</sub>, AsF<sub>3</sub>) determined at low pressure (<1 bar) in a water-free system. However, water represents

from 90 to 99% of volcanic gas and fumarolic vapor compositions. A few experiments evidenced that hydroxide and hydrated metal species (e.g., H<sub>2</sub>MoO<sub>4</sub>, Belton and Jordan, 1965; Ca(OH)<sub>2</sub>, Al(OH)<sub>3</sub>, Si(OH)<sub>4</sub>, Hashimoto, 1992) can be dominant at volcanic temperatures even at water pressures of 1 bar. These still scarce data imply an important role of the solvent (water) in the vapor speciation of metals and thus require systematic experimental studies for As and other elements.

The goal of this study was to obtain new information on the identity and stability of As species existing in natural vapors and low-density supercritical aqueous fluids. For this purpose, vapor/solid (As<sub>2</sub>O<sub>3</sub>) and vapor/aqueous solution (H<sub>2</sub>O–NaCl) partition coefficients for As were measured as a function of water pressure and H<sub>2</sub>S, HCl, and NaCl content up to 450°C. Extended X-ray absorption fine structure spectroscopic measurements were performed in situ on As<sub>2</sub>O<sub>3</sub>–H<sub>2</sub>O–NaCl solutions in a wide range of temperatures (30 to 500°C) and solvent densities (0.1 to 1.1 g cm<sup>–3</sup>). The results were used to generate thermodynamic parameters for As<sup>(III)</sup> and As<sup>(V)</sup> hydroxide gaseous species and to predict As speciation and fractionation in boiling hydrothermal systems and volcanic gases.

## 2. EXPERIMENTAL

### 2.1. As<sub>2</sub>O<sub>3</sub> Vapor-Phase Solubility and Arsenic Vapor–Liquid Partitioning Measurements

#### 2.1.1. Experimental materials and conditions

Measurements of As<sup>(III)</sup> partitioning between aqueous solution (As–H<sub>2</sub>O  $\pm$  NaCl  $\pm$  NaOH  $\pm$  HCl  $\pm$  H<sub>2</sub>S) and its saturated vapor were conducted with aqueous arsenious acid (H<sub>3</sub>AsO<sub>3</sub>) solutions of concentration ranging from 0.0001m As to the saturation with respect to As<sub>2</sub>O<sub>3</sub> solid (>10m), at saturated vapor pressure of the system (P<sub>sat</sub>). The following solution compositions and temperatures were investigated: pure water at 250, 300, and 350°C; H<sub>2</sub>O–NaCl solutions at 300, 350, 400, and 450°C; and H<sub>2</sub>O–H<sub>2</sub>S, H<sub>2</sub>O–HCl, and H<sub>2</sub>O–NaOH at 350°C (Tables A1 to A4 of the Appendix). Several measurements were also conducted with aqueous solutions of arsenic acid (H<sub>3</sub>As<sup>(V)</sup>O<sub>4</sub>) at 350°C with As<sup>(V)</sup> aqueous concentrations from 0.005 to 0.05m (Table A5 of the Appendix).

Arsenious and arsenic acid solutions were prepared by dissolving, respectively, As<sub>2</sub>O<sub>3</sub> and As<sub>2</sub>O<sub>5</sub> solids (Merck Normapur) in deionized, degassed H<sub>2</sub>O. Sodium chloride salt, or 1m HCl or 1m NaOH solutions (Normapur) were added by weight in the As solutions to desired concentrations. To avoid possible As oxidation in the experiments with As(III), solutions were flushed for  $\sim 30$  min with argon or hydrogen gas before loading into the reactor. Hydrogen sulfide was introduced in the reactor as aluminum sulfide (Al<sub>2</sub>S<sub>3</sub>, Normapur), which produces H<sub>2</sub>S and Al hydroxide when reacting with water.

Measurements of As vapor–solid partitioning were performed on arsenolite (cubic As<sub>2</sub>O<sub>3</sub>) at 130, 220, 250, 265, and 300°C as a function of water pressure ranging from 0 to P<sub>sat</sub>. Although at these conditions arsenolite is considered to be thermodynamically metastable with respect to the monoclinic As<sub>2</sub>O<sub>3</sub> polymorph claudetite (Schulman and Schumb, 1943; Pokrovski et al., 1996), all attempts to synthesize the necessary quantity of this monoclinic phase have failed. Arsenolite was always found to rapidly form in the presence of aqueous solution or water vapor. This was in agreement with previous studies that reported a very slow kinetics of arsenolite-to-claudetite transition, and, by contrast, the extreme facility for arsenolite to form in the system As<sub>2</sub>O<sub>3</sub>–H<sub>2</sub>O (e.g., Rushton and Daniels, 1926; Schulman and Schumb, 1943). Consequently, arsenolite was chosen for measurements to 300°C in the present study. Arsenolite was synthesized via the dissolution of As<sub>2</sub>O<sub>3</sub> in oxygen-free H<sub>2</sub>O at 200°C, followed by a slow cooling to ambient temperature. Because arsenolite melts between 275 and 315°C (Rushton and Daniels, 1926), measurements at 350°C were performed with molten As<sub>2</sub>O<sub>3</sub>. The molten phase was obtained directly in the experiment from As<sub>2</sub>O<sub>3</sub> solid placed in the reactor. The complete

$\text{As}_2\text{O}_3$  melting was inferred from both the measured solubilities (see below), and optical and X-ray diffraction analyses of the quenched solid products after experiment, which showed the only presence of glassy  $\text{As}_2\text{O}_3$ . Vapor–solid partitioning measurements were conducted via two complementary techniques (Tables A6 and A7 of the Appendix), allowing either rapid quenching at the end of the experiment or in situ sampling of the vapor phase. Vapor–liquid partitioning experiments were performed with a sampling technique (see below).

### 2.1.2. Quenching technique

Dissolution experiments of arsenolite in undersaturated water vapor at 130, 220, 265, and 300°C were performed in  $\sim 40\text{ cm}^3$  titanium-alloy (VT-8) reactors held in an air-thermostated oven (SNOL-3.5M). Temperature gradients were minimized to less than 0.1°C per autoclave height by placing a wall-thick copper cylinder into the oven. Details about the experimental equipment and procedure were similar to those described by Migdisov et al. (1998), Migdisov et al., (1999) and Archibald et al. (2001). A 7-cm-long, 0.5-cm-inner-diameter Pyrex ampoule opened at its top that contained 0.5 to 1 g of dry solid was placed into the autoclave. A weighed amount of deionized and degassed water was introduced with a syringe at the bottom of the reactor outside the ampoule. The reactor volume was determined before experiments, both geometrically from the reactor and ampoule dimensions and by filling with pure water at controlled temperature ( $22 \pm 1^\circ\text{C}$ ). Pressure was estimated from the reactor free volume and loaded amount of water according to the PVT properties of pure water vapor (Kestin et al., 1984); we assumed that the low concentrations of As in the vapor did not significantly modify these properties. At the end of the run, the reactor was quenched in cold water for 15 min, the Pyrex ampoule was weighed, and the  $\text{As}_2\text{O}_3$  solid and water condensed on the reactor walls and bottom were washed with a weighed amount of 0.1M NaOH solution, which was then analyzed for As (see below). The ampoule was dried at 105°C during a few hours and weighed again. Arsenic quantity dissolved in the vapor, calculated from the ampoule weight loss and from analyses of the washing solution, was always the same, in the limit of  $\pm 10\text{ wt\%}$  of the value. As demonstrated in this (see below) and previous studies (Migdisov et al., 1998, Migdisov et al., 1999; Zakaznova-Iakovleva et al., 2001), the quenching technique can be effectively used for studying vapor–solid equilibria in simple systems involving solids easily condensable on cooling.

### 2.1.3. Sampling technique

In the case of vapor–liquid coexistence, a rapid irreversible redistribution of the solute and solution (condensation on colder parts of the reactor, boiling of the solution) occurs during both heating and cooling. This inevitably results in poor reproducibility and overestimation of the solubility in the vapor phase (Alekhin and Vakulenko, 1988; Migdisov et al., 1999). Therefore, the quenching technique described above could not be used for vapor–liquid partition measurements. Consequently, all vapor–liquid partition measurements, and also some vapor-phase  $\text{As}_2\text{O}_3$  solubility experiments (at 250 and 350°C), were performed with a specially developed reactor. The experimental technique is modified after that described in Zakirov and Sretenskaya (1994). The method allows both in situ separation of a part of the vapor phase at the end of the experiment and extraction of vapor samples through a capillary tubing during the run. The experimental apparatus consists of a  $\sim 100\text{-cm}^3$  internal volume Ti-alloy (VT-8) pressure vessel (Fig. 1) placed in a  $\sim 80\text{-cm}$ -height vertical furnace. Temperature is maintained within  $\pm 0.2^\circ\text{C}$  by two heating resistances independently regulated by a Eurotherm-900HP programmer and K-type (Chromel-Alumel) thermocouples. Vertical temperature gradients were minimized in an empty reactor before experiments by adjusting the electric power of each resistance so that they did not exceed 0.3°C per autoclave height ( $\sim 30\text{ cm}$ ). An opening on the vessel top was connected to sampling valve and pressure transducer via titanium and 316SS capillary tubing. Dead volumes of the pressure and sampling lines were  $0.6\text{ cm}^3$ . Pressure was measured with a P60 tensor transducer manufactured at the Institute NII-TEPLOPRIBOR (Moscow) and connected to a Keithley-2000 multimeter. The reproducibility of measurement at maximum experimental pressure ( $\sim 300\text{ bar}$ ) was within 1 bar. In the upper part of the vessel was fixed a  $\sim 10\text{ cm}^3$  cylindrical rigid Ti ampoule with a cover fitted to

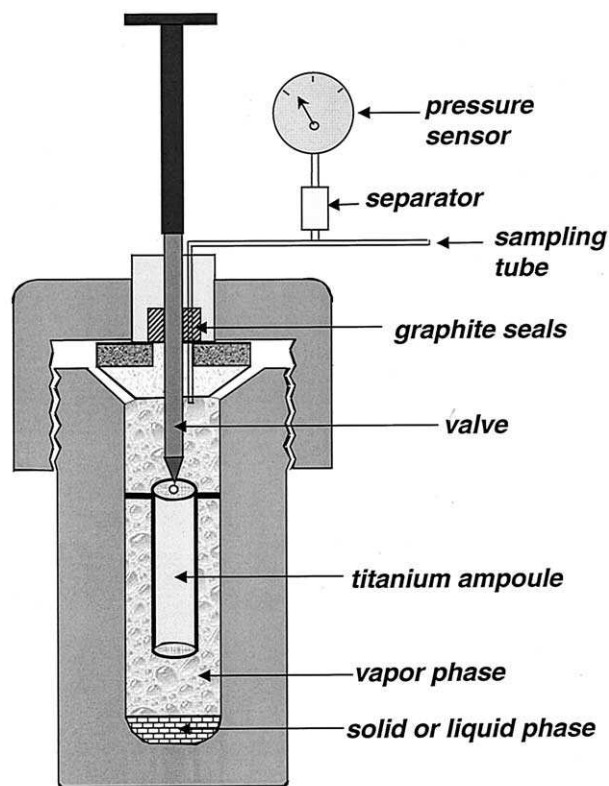


Fig. 1. Schematic drawing of the titanium-alloy reactor used for vapor–liquid and vapor–solid partitioning measurements.

the ampoule body via a platinum ring seal. The ampoule can be tightly closed, through a hole in its cover, via a valve fitted in the vessel obturator. Graphite-based (Cefigraf) seals around the stem allow the valve operation during experiment without fluid leakage. The free volumes of the equipped vessel and ampoule were determined by filling with deionized degassed water (section 2.1.2). They were assumed to not change in the limit of their uncertainties ( $\pm 0.5\%$ ) at experimental temperature and pressure. The charged vessel and ampoule were accurately weighed before and after each experiment to assure nothing was lost to leakage.

In the beginning of the experiment, weighed experimental solution (20 to 40 g) or solid  $\text{As}_2\text{O}_3$  (0.5 to 1.5 g) with necessary amount of water were placed at the bottom of the reactor. At the run temperature, the solution did not enter the ampoule, which is situated in the upper part of the reactor occupied by the vapor phase and kept closed by the valve (Fig. 1). During vapor–liquid partitioning experiments at  $\geq 300^\circ\text{C}$ , samples of vapor condensate were periodically taken via the capillary tubing. Two to four successive aliquots of 0.3 to 0.7 g each were withdrawn in every sampling session. They were weighed, diluted (if necessary), and analyzed for As, Na, and pH (see below). The first aliquot of the condensate, which served to wash the sampling capillary, was usually rejected. No systematic variations of metal concentrations and pH were recorded in the following samples. At the end of the experiment, the ampoule was gently opened to minimize the rate of pressure drop as a result of volume increase, which could result in a rapid adiabatic fluid expansion and consequently a decrease in temperature, vapor recondensation, or solution boiling. The ampoule remained open for 10 to 60 min to equilibrate the system and was then closed; the reactor was then taken out of the furnace and cooled to room temperature by compressed air. The ampoule was weighed, opened, and washed with  $\text{H}_2\text{O}$  or  $\text{H}_2\text{O-NaOH}$  solutions to remove all the solid and liquid condensed on its walls. The mass of water condensate trapped in the ampoule always matched, within 10%, the calculated mass using the ampoule volume and water vapor density at the given temperature and pressure.

Arsenic concentrations determined after the experiment in the residue of the liquid phase (if present) from the reactor corresponded to the limit of 5% to their counterparts calculated from the initial solution concentrations and mass of vapor samples, demonstrating that no loss of As, other than through sampling, occurred during the experiments. Arsenic vapor concentrations for similar solutions measured after both sampling via capillary ("extraction technique") and trapping into the ampoule ("ampoule technique") were always close to one another (Tables A1, A2, and A4 of the Appendix). This demonstrates that both methods were adequate for vapor-liquid fractionation studies for at least relatively soluble elements (As) and vapor densities higher than  $0.04 \text{ g cm}^{-3}$  (see below).

At lower densities, corresponding to the undersaturated water vapor or vapor-liquid equilibrium at temperatures lower than  $300^\circ\text{C}$ , the quantity of the vapor phase in the reactor ( $<2$  to  $3 \text{ g}$ ) was too small to be accurately sampled via capillary. Consequently, vapor-liquid partition runs at  $250^\circ\text{C}$  and  $\text{As}_2\text{O}_3$  solubility experiments in undersaturated water vapor at  $250$  and  $350^\circ\text{C}$  were conducted using only the ampoule technique (Table A6 of the Appendix).

#### 2.1.4. Analytical methods and vapor-liquid composition calculations

Arsenic concentrations in sampled or quenched vapor condensates as well as aqueous solutions before and after the experiment were measured by atomic absorption spectroscopy (AAS) with acetylene-air flame (Pokrovski et al., 2002a), colorimetry with the arsenic molybdate blue complex (Marczenko, 1986; modified by Pokrovski, 1996), and titration with iodine (Charlot, 1966), depending on As content in the experiments. Details about these analytical techniques are described elsewhere (Pokrovski, 1996; Pokrovski et al., 2002a). Combination of these methods allows accurate analyses ( $\pm 2\%$ ) of both total As (AAS and colorimetry) and  $\text{As}^{\text{V}}$  (colorimetry) and  $\text{As}^{\text{III}}$  (titration) in a wide concentration range (from  $0.01$  to  $10000 \text{ ppm As}$ ). Arsenic concentrations of the same experimental solutions analyzed by the three methods were always the same within  $\pm 5\%$ .

Sodium concentrations in the condensates from selected NaCl-rich experiments were measured in the range  $0.02$  to  $10 \text{ ppm}$  via acetylene-air flame emission spectroscopy at an emission line of  $589 \text{ nm}$  with a reproducibility of  $\pm 5\%$  and a detection limit of  $0.01 \text{ ppm Na}$ . Values of pH were measured at ambient temperature ( $20 \pm 2^\circ\text{C}$ ) with a combination pH glass electrode calibrated on the activity scale using the National Institute of Standards and Technology (NIST) tartrate, phthalate, phosphate, and borate buffers ( $\text{pH}_{20^\circ\text{C}} = 1.69, 4.00, 6.87$  and  $9.21$ , respectively) and  $0.1 \text{ M HCl}$  and  $0.01 \text{ M NaOH}$  solutions ( $\text{pH}_{20^\circ\text{C}} = 1.10$  and  $12.10$ , respectively).

Sodium vapor-phase concentrations measured in the system  $\text{H}_2\text{O-NaCl-As}$  using the sampling through capillary at  $300$  and  $350^\circ\text{C}$  were found to be in reasonable agreement with data available in the literature (see compilation of Bischoff and Pitzer, 1989). For example, the average NaCl concentration in the vapor in equilibrium with a  $\sim 4 \text{ molal NaCl}$  solution at  $350^\circ\text{C}$  measured in this study,  $\sim 0.0004 \text{ m}$  (Table A4), is close to the corresponding value reported by Bischoff and Pitzer (1989),  $\sim 0.0005 \text{ m}$ . At higher temperatures, however, the sampling gives values usually lower by a factor of  $5$  to  $10$  than most of the data cited in the literature. This discrepancy likely arises from the possible NaCl precipitation in the cold capillary tubing during sampling in the present study. This is confirmed by the fact that a few measurements carried out in this study at  $400$  and  $450^\circ\text{C}$  by the ampoule technique, which avoids temperature gradients and thus irreversible fractionations (section 2.1.3), have provided vapor NaCl concentrations close to the literature data in the limit of  $\pm 30\%$  of the value (Table A4). The values of pH measured in both vapor condensates and liquid from experiments in the  $\text{H}_2\text{O-NaCl-As(III)}$  system were essentially neutral, indicating that the hydrolysis of NaCl to produce NaOH and HCl is not important up to at least  $450^\circ\text{C}$ , in agreement with previous studies (Bischoff et al., 1986).

Arsenic, NaCl, and NaOH equilibrium concentrations in the liquid phase at each sampling were calculated via the mass balance from the initial solution composition and amount, measured As and Na concentrations in the vapor phase, and the amount of samples taken. The estimation of the masses of vapor and liquid at equilibrium, necessary for calculation of the liquid-phase concentrations, requires knowledge of the vapor and liquid densities and the reactor volume. The density of

the vapor phase was derived from the pressure measured before each sampling with the PVT properties of pure water (Kestin et al., 1984) and assuming that small amounts of As, NaCl, or  $\text{H}_2\text{S/HCl}$  in the vapor (mole fraction  $<0.01$ ) do not significantly modify these properties. The vapor densities calculated via this approach in the system  $\text{NaCl-H}_2\text{O}$  at  $350$  to  $450^\circ\text{C}$  were identical, in the limit of  $\pm 5\%$ , to those reported by Khaibullin and Borisov (1966) and Bischoff (1991). The liquid-phase densities for  $\text{H}_2\text{O-As-HCl-H}_2\text{S}$  dilute solutions were assumed to be equal to those of pure water, and those for  $\text{H}_2\text{O-NaCl}$  solutions were taken from the compilation of Bischoff (1991). For vapor-liquid partitioning experiments carried out on  $\text{H}_2\text{O-NaCl-As}$  solutions, the measured pressures and derived NaCl liquid-phase concentrations were in reasonable agreement with the composition-pressure two-phase equilibrium curve for the system  $\text{H}_2\text{O-NaCl}$  reported in previous studies (Bischoff and Pitzer, 1989, and references therein).

Vapor-phase concentrations of hydrochloric acid in  $\text{H}_2\text{O-HCl-As}$  experiments were determined from the pH of the vapor condensates. The corresponding liquid-phase HCl concentrations were calculated via the mass balance and the density approximations as discussed above. The obtained HCl vapor/liquid partition coefficients were in good agreement with those measured by Simonson and Palmer (1993). Vapor- and liquid-phase concentrations of hydrogen sulfide in  $\text{H}_2\text{O-H}_2\text{S-As}$  experiments were calculated via the mass balance as described above and  $\text{H}_2\text{S}$  Henry constants reported by Suleimenov and Krupp (1994).

## 2.2. X-Ray Absorption Spectroscopy Spectroscopy

X-ray absorption spectroscopy (XAFS) (including the X-ray absorption near edge structure region or XANES, and extended X-ray absorption line structure or EXAFS) was performed on  $\sim 0.3 \text{ m H}_3\text{AsO}_3$  ( $\pm \text{NaCl}$ ) aqueous solutions prepared at described above (section 2.1.2), at temperatures from  $30$  to  $500^\circ\text{C}$  and pressures  $250$  and  $600 \text{ bar}$ . The spectra were collected in transmission mode at the As K-edge ( $\sim 11870 \text{ eV}$ ) over the energy range  $11800$  to  $12800 \text{ eV}$ , at the collaborative research group IF BM32 beam line at the European Synchrotron Radiation Facility (ESRF; Grenoble, France). The storage ring was operated in the multibunch filling mode at  $6 \text{ GeV}$  with  $100$  to  $200 \text{ mA}$  current. The beam energy was selected with a Si(111) double crystal monochromator with sagittal focusing. The focusing at BM32 beam line allows to reduce the beam size on the sample to  $\sim 0.3 \times 0.3 \text{ mm}$  while keeping a high X-ray photon flux ( $\sim 10^{13}$  photons/s per sample).

Experimental solutions were placed in a special high-pressure cell developed at the Laboratoire de Cristallographie (Grenoble, France). Details about cell construction and handling can be found elsewhere (Tamura et al., 1995; Soldo et al., 1998). The apparatus consists of a polycrystalline sapphire optical cell (Fig. 2a) that is inserted in a super high tension steel vessel. The vessel has a water-cooling jacket and two Be windows for X-ray passage (Fig. 2b). The sapphire cell contains two inner tubes, each having one closed and polished end ( $\sim 0.15 \text{ mm}$  of thickness) and an outer coaxial tube. The experimental solution is placed in a gap between the two polished ends, which serve as X-ray windows. The thickness of the sample space is adjusted so that the jump in X-ray absorption at the absorption edge was about unity. The cell has a sample reservoir attached to the end of the outer tube. The reservoir and the sample space are connected through a narrow channel between the inner and outer tubes. The temperature in the sample space is maintained by Mo heating resistances and Pt-Pt/Rh thermocouples connected to a Eurotherm temperature regulator. The cell is pressurized by high-purity grade helium gas with low absorption constant for X-rays. Pressure in the sample space is always balanced with that of He gas through the liquid surface in the reservoir. Thus, the sample thickness is kept constant at high T and P, and thin sapphire walls are never broken by stress. This design permits operation at up to  $2000^\circ\text{C}$  and  $2 \text{ kbar}$ .

Because the length ( $\sim$ volume) of the sample space always remains constant, with increasing temperature at constant pressure, the solution in the sample space expands into the reservoir. The absorption jump of a spectrum in such cell configuration is proportional to the fluid density times absorber (As) concentration per unit mass of fluid. It was found that the change in the absorption jump with temperature (and pressure), both on heating and cooling, closely follows that of the fluid density (assumed to be equal to that of pure water or NaCl- $\text{H}_2\text{O}$  solutions; see

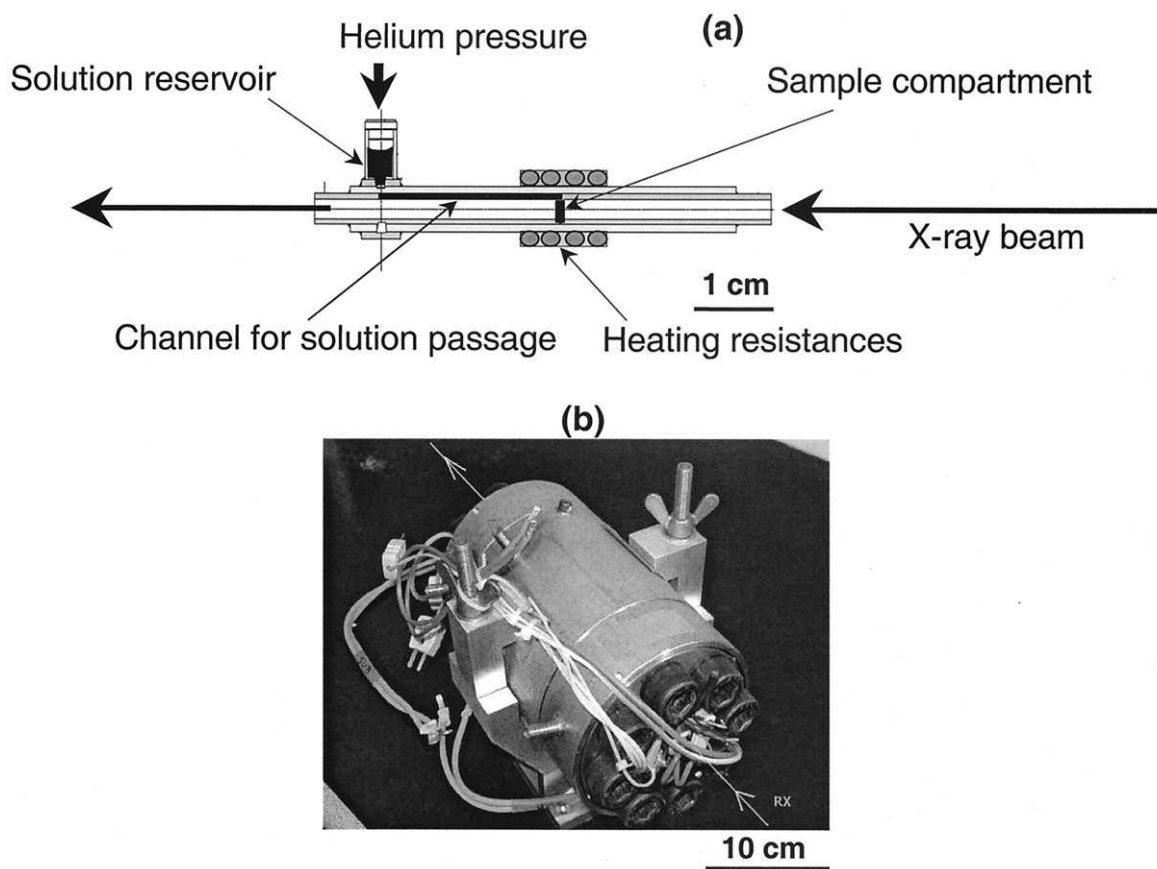


Fig. 2. (a) Schematic drawing of an optical cell used for XAFS measurements. (b) Photograph of the pressure vessel mounted at BM32 beam line of the ESRF.

above). This demonstrates that neither loss of the solution occurs via evaporation through the sample reservoir nor precipitation of As-bearing phases takes place in the sample space or channel.

Spectra acquisition and analysis were similar to those described in Pokrovski et al. (2000), Pokrovski et al., (2002b). To obtain the necessary signal-to-noise ratio, three to six scans (of  $\sim 1$  h per scan) at each temperature for each solution were performed up to high  $k$  values ( $\sim 15 \text{ \AA}^{-1}$ ). After acquisition, all scans were carefully inspected, and if they were found to be reasonably free of beam intensity fluctuations and other flaws, they were added together.  $\text{As}_2\text{O}_3$  (cubic and glassy),  $\text{NaAsO}_2$ ,  $\text{As}_2\text{O}_5$ , and  $\text{Na}_2\text{HAsO}_4 \cdot 7\text{H}_2\text{O}$  solids, which serve as model compounds for As local environment, were recorded in the transmission mode at ambient temperature. XAFS data analysis was performed by the SEDEM (Aberdam, 1998) and XAFS2.6 (Winterer, 1997) software packages, following the standard procedure (Teo, 1986). The structural information about As atomic environment (identity of first and second (if present) neighbor atoms, distances between As and their neighbors, average coordination numbers, and the Debye-Waller factors) was obtained from the least-square fit of the raw EXAFS spectrum or inverse Fourier transform for each atomic shell. Backscattering amplitude and phase-shift functions were extracted from the solid references for As-O or computed by the FEFF 6.01 ab initio code (Zabinsky et al., 1995; Ankudinov and Rehr, personal communication) for As-As, As-Na, and As-Cl pairs. The influence of the self-absorption and disorder (thermal and static) on determining accurate structural parameters was tested by use of the cumulant expansion method (e.g., Farges et al., 1996; Soldo et al., 1998). Possible multiple scattering phenomena within the first As coordination shell were also checked by using the FEFF 6.01 code. Self-absorption, disorder, and multiple scattering phenomena were found to be too weak to significantly affect As structural parameters. Explicit account for the temperature–pressure evolution of these contributions will be provided elsewhere later.

### 3. RESULTS AND DISCUSSION

#### 3.1. XAFS Spectroscopy

XANES of all As-bearing solutions (data not shown) exhibit shapes and edge-crest positions close to those of arsenolite,  $\text{As}_2\text{O}_3$ -glass and sodium arsenite ( $\text{NaAsO}_2$ ). This suggests a valence state +3 for arsenic in solution, and likely a pyramidal configuration with three oxygen neighbors in the first atomic shell of arsenic, similar to those in these solids (Loehr and Plane, 1968; Pertlik, 1978). No changes in shape and edge energy that could indicate the presence of arsenate ( $\text{As}^{5+}\text{O}_4$ ),  $\text{As}(\text{aq})$ , or  $\text{H}_3\text{As}(\text{aq})$  were observed at any temperature and pressure for a run duration up to 2 d. This demonstrates that neither As oxidation nor reduction occurred in our experimental solutions.

Normalized EXAFS spectra and their corresponding Fourier transforms for  $\sim 0.3\text{m}$  arsenious acid aqueous solutions ( $\pm 10$  wt% NaCl) at 250 and 600 bar as a function of temperature are reported in Figures 3 and 4. The derived structural parameters (distances, number of neighbors, degree of disorder) are summarized in Table 1. All spectra exhibit a single contribution from the oxygens of the first As atomic shell. Modeling these spectra gives  $3 \pm 0.3$  oxygens in the first shell with a mean As-O distance of  $1.78 \pm 0.01 \text{ \AA}$  in the temperature range 30 to  $500^\circ\text{C}$ . This is consistent with the predominance of the

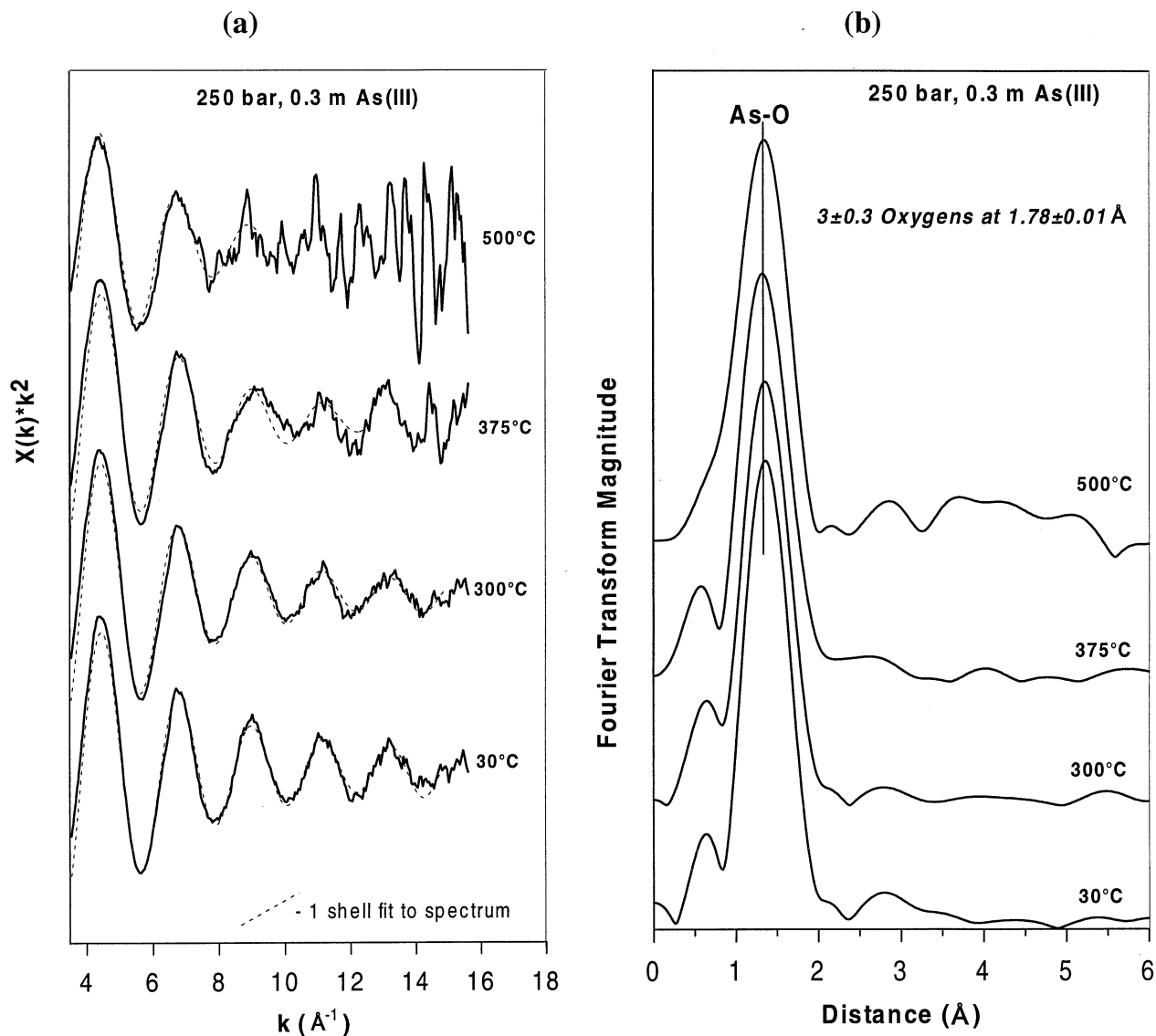


Fig. 3.  $k^2$ -weighted EXAFS spectra at As K-edge of a 0.3-*m* arsenious acid aqueous solution at 250 bar and indicated temperatures (a) and their corresponding Fourier transforms (b). Dashed curves represent single-shell fit to the total EXAFS spectrum; solid vertical line indicates the first As atomic shell, composed of three oxygens in the  $\text{As}(\text{OH})_3$  complex. No changes in As-O distances were detected from 30 to 500°C. The high noise associated with the spectrum at 500°C is due to the decrease of the fluid density (by 10 times in comparison with 30°C).

$\text{As}(\text{OH})_3^\circ$ , in agreement with the previous Raman spectroscopy and solubility studies (Loehr and Plane, 1968; Pokrovski et al., 1996; Gout et al., 1997). The spectra of As(III) aqueous solutions at 250 and 600 bar are very similar at all temperatures, suggesting that the  $\text{As}(\text{OH})_3$  structure remains the same both in high-density aqueous solution and low-density supercritical fluid ( $0.1 \text{ g cm}^{-3} \leq \text{density} \leq 1.1 \text{ g cm}^{-3}$ ; Table 1). The structural parameters derived from the spectra of the 10 wt%  $\text{NaCl-H}_3\text{AsO}_3$  fluid at 600 bar are identical, in the limit of their uncertainties, to those of its pure water analog. This demonstrates the absence of significant (>10%) amounts of As chloride or hydroxy-chloride inner-sphere complexes, in agreement with thermodynamic calculations (Heinrich and Eadington,

1986; Pokrovski et al., 2002a). No second shell contributions that could arise from neighboring As in polymeric species, Na, or Cl presented in outer-sphere complexes, nor were oxygens from the water hydration sphere detected. Note that the As-O distances changed very little as temperature increased (in the limit of 0.01 Å from 30 to 500°C). This behavior is similar to that of other strongly bound OH/O aqueous complexes such as molybdate ( $\text{MoO}_4^{2-}$ ) and wolframate ( $\text{WO}_4^{2-}$ ), which also exhibit only minor changes in their metal-oxygen distances (within 0.01 Å) in a wide temperature range (Mosselmans et al., 1996; Hoffmann et al., 2000). Strongly hydrated cations (e.g.,  $\text{Ag}^+$ ,  $\text{Sr}^{2+}$ ; Seward et al., 1996, Seward et al., 1999) and aqueous neutral or charged complexes with a more ionic char-

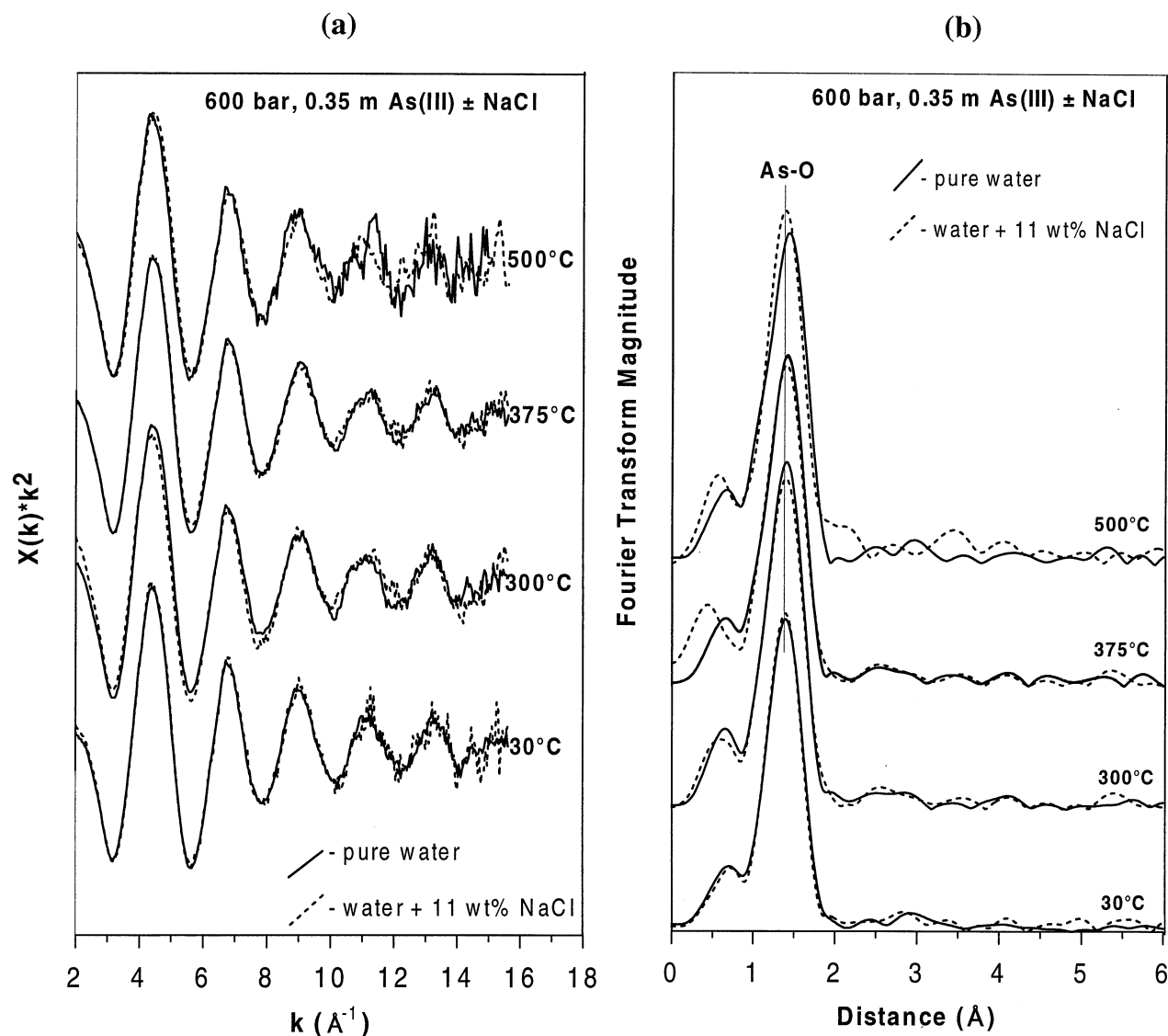


Fig. 4.  $k^2$ -weighted EXAFS spectra at As-K edge of  $\sim 0.35$ -M arsenious acid aqueous solutions with and without NaCl at 600 bar and indicated temperatures (a) and their corresponding Fourier transforms (b). The vertical line in Fig. 4b denotes the first As atomic shell composed of three oxygens. No detectable changes in the number of neighbors ( $\leq 0.5$  atoms) and As-O average distances ( $\leq 0.01$   $\text{\AA}$ ) occur from 30 to 500°C.

acter (e.g.,  $\text{SbCl}_{3-4}$ , Oelkers et al., 1998;  $\text{CuCl}_{2-3}$ , Collings et al., 2000;  $\text{ZnBr}_{3-4}$ , Mayanovic et al., 2001) demonstrate, by contrast, significant shortening of the hydration shell radius and metal-ligand bond length with increasing temperature, typically  $\sim 0.10$   $\text{\AA}$  in the range 25 to 300°C. This contraction is in agreement with the temperature changes in solvent-solute interactions, including such factors as dielectric saturation and solvent compressibility (e.g., Shock et al., 1992; Oelkers et al., 1998). Thus, the constancy of the As-O bond length over the wide temperature (30 to 500°C) and density range (1.1 to 0.1  $\text{g cm}^{-3}$ ) implies that as a result of a strong covalent character of the As-OH bonds (Pauling, 1948) and the absence of significant hydration around the  $\text{As}(\text{OH})_3^\circ$  molecule or interactions with Na and Cl, the increased thermal vibration with temperature has no significant effect on the interatomic distances and the structure of the first As atomic shell.

### 3.2. Arsenic Vapor-Liquid Partitioning

Detailed information about the arsenic vapor-liquid partitioning measurements performed in this study for different systems as a function of As, HCl,  $\text{H}_2\text{S}$ , NaCl, and NaOH concentrations is presented in Tables A1 to A5 of the Appendix, and the average data for a given temperature and system composition are summarized in Table 2. In this article, arsenic vapor-liquid partition coefficient,  $K_m$ , is defined as the ratio of As concentration in the vapor (mol/kg of vapor) and liquid phase (mol/kg of solution) in equilibrium:

$$K_m = m_{\text{As, vapor}}(\text{mol/kg})/m_{\text{As, liquid}}(\text{mol/kg}). \quad (1)$$

Note that in dilute (As < 1m)  $\text{H}_2\text{O}$  solutions, this equation corresponds to the conventional molality units (mol/kg  $\text{H}_2\text{O}$ ). In highly concentrated solutions and in the presence of signif-

Table 1. Structural parameters of the first arsenic–oxygen atomic shell obtained from fitting As K-edge EXAFS spectra of As(III)-bearing aqueous fluids recorded as a function of pressure and temperature.<sup>a</sup>

Solution composition	P (bar)	T (°C)	Fluid density (g cm <sup>-3</sup> )	Fitted k range (Å <sup>-1</sup> )	N <sub>As-O</sub> (atom)	R (Å)	σ <sup>2</sup> (Å <sup>2</sup> )	χ <sup>2</sup>
0.30m H <sub>3</sub> AsO <sub>3</sub>	250	30	1.00	3.0–15.0	3.0	1.78	–0.0003	0.13
	250	300	0.74	3.0–14.6	3.2	1.78	0.0008	0.10
	250	375	0.51	3.0–13.5	3.3	1.78	0.0018	0.14
	250	500	0.09	3.0–10.0	3.3	1.78	0.0050	0.18
0.35m H <sub>3</sub> AsO <sub>3</sub>	600	30	1.02	3.0–14.9	3.2	1.78	0.0002	0.11
	600	300	0.79	3.0–14.9	3.3	1.79	0.0010	0.10
	600	375	0.67	3.0–14.7	3.5	1.78	0.0016	0.13
	600	500	0.21	3.0–14.5	3.2	1.79	0.0060	0.14
0.35m H <sub>3</sub> AsO <sub>3</sub> +1.8m NaCl	600	30	1.10	3.0–14.5	3.0	1.78	–0.0005	0.12
	600	300	0.90	3.0–14.9	2.9	1.78	0.00006	0.11
	600	375	0.79	3.0–14.9	3.0	1.78	0.0003	0.10
	600	500	0.56	3.0–14.5	3.2	1.78	0.0004	0.15
					±0.3	±0.01	±0.0003	

<sup>a</sup> Concentrations are expressed in mol/kg of solution (m); densities for H<sub>2</sub>O–H<sub>3</sub>AsO<sub>3</sub> and H<sub>2</sub>O–H<sub>3</sub>AsO<sub>3</sub>–NaCl solutions were approximated respectively by those for pure water (Kestin et al., 1984) and for H<sub>2</sub>O–NaCl (Potter and Brown, 1977). R = arsenic–oxygen mean distance; N = As–O coordination number; σ<sup>2</sup> = squared Debye–Waller factor (relative to the first shell of As<sub>2</sub>O<sub>3</sub>(cub) solid at ambient temperature and pressure); χ<sup>2</sup> = D/(F × M) × Σ(Y<sub>exp</sub><sup>2</sup> – Y<sub>fit</sub><sup>2</sup>), where D = number of independent data, F = degrees of freedom, M = number of data points fitted, and Y<sub>exp</sub><sup>2</sup> – Y<sub>fit</sub><sup>2</sup> = difference between experimental and fitted squared EXAFS absorption coefficient (k<sup>2</sup>·X) of the raw signal for each point (Press et al., 1986).

Values in the last row represent average uncertainties for R, N, and σ<sup>2</sup>.

icant amounts of salt (NaCl), the use of the molality scale is more ambiguous because H<sub>2</sub>O activity becomes very different from 1. Consequently, in the present study, we decided to use the more universal partition coefficient defined by Eqn. 1.

It can be seen in Tables A1 to A5 that the values of K<sub>m</sub> at a given temperature and similar solution compositions obtained by sampling through capillary or trapping into the ampoule are the same in the limit of their uncertainties. This demonstrates the validity of both techniques for studying As vapor solubilities in a wide range of temperature (at least from 250 to 450°C) and vapor density (at least from 0.005 to 0.20 g cm<sup>-3</sup>). The values of K<sub>m</sub> obtained at 250 and 300°C for similar As liquid concentrations are independent of the run duration longer than a day or two, thus suggesting a rapid attainment of equilibrium for As between solution and vapor. At higher temperatures, the equilibrium was considered to be attained within a few hours. The results on As vapor–liquid partitioning are discussed below for each system.

### 3.2.1. Pure water

The data on As(III) partition between H<sub>3</sub>AsO<sub>3</sub>–H<sub>2</sub>O solution and its saturated vapor at 250, 300, and 350°C are presented in Table A1 of the Appendix. In Figure 5, arsenic concentrations in the vapor phase are plotted vs. their corresponding liquid-phase contents. It can be seen in this figure that at low to moderate As liquid-phase contents (up to ~1m), measured equilibrium vapor-phase As concentrations are linearly proportional to their corresponding liquid-phase concentrations. The slopes (in log scale), at all temperatures investigated, are equal to 1 in the limit of the uncertainties (Fig. 5). As was shown by XAFS spectroscopy in the present study and by previous Raman spectroscopy and solubility measurements (Pokrovski et al., 1996; Gout et al., 1997), the monomeric As(OH)<sub>3</sub> complex entirely dominates arsenic speciation in aqueous solution of arsenious acid to ~1m at temperatures higher than 200°C. As a result, the same monomeric species As(OH)<sub>3</sub> is likely to form

Table 2. Average vapor/liquid partition coefficients for As(III) and As(V) in dilute (<1m As) H<sub>2</sub>O, H<sub>2</sub>O–HCl, and H<sub>2</sub>O–H<sub>2</sub>S solutions; Henry constants of reactions 2 and 3; and standard molal Gibbs free energies of As(OH)<sub>3</sub>(gas) and AsO(OH)<sub>3</sub>(gas) at corresponding temperature at P<sub>sat</sub>.

T (°C)	Solution composition	Average vapor/liquid partition coefficient, (K <sub>m</sub> )	Henry constant, K <sub>h</sub> (bar/mol/kg)	ΔG <sup>o</sup> <sub>T,P<sub>sat</sub></sub> <sup>a</sup> (kJ/mol)
250	H <sub>3</sub> AsO <sub>3</sub> –H <sub>2</sub> O	0.012 ± 0.003	0.0084	–677.9 ± 4.2
300	H <sub>3</sub> AsO <sub>3</sub> –H <sub>2</sub> O	0.063 ± 0.020	0.097	–703.6 ± 5.6
350	H <sub>3</sub> AsO <sub>3</sub> –H <sub>2</sub> O	0.145 ± 0.020	0.432	–727.1 ± 6.7
350	H <sub>3</sub> AsO <sub>3</sub> –H <sub>2</sub> O–HCl(≤0.1 m)	0.165 ± 0.015	—	—
350	H <sub>3</sub> AsO <sub>3</sub> –H <sub>2</sub> O–H <sub>2</sub> S(≤0.5 m)	0.146 ± 0.037	—	—
350	H <sub>3</sub> AsO <sub>4</sub> –H <sub>2</sub> O	0.039 ± 0.006	0.116	–830.9±? <sup>b</sup>

<sup>a</sup> Calculated from the values of K<sub>h</sub> and using the thermodynamic properties for As(OH)<sub>3</sub>(aq) and AsO(OH)<sub>3</sub>(aq), respectively, from Table 4 and Shock et al. (1997).

<sup>b</sup> Uncertainty of this value is unknown.

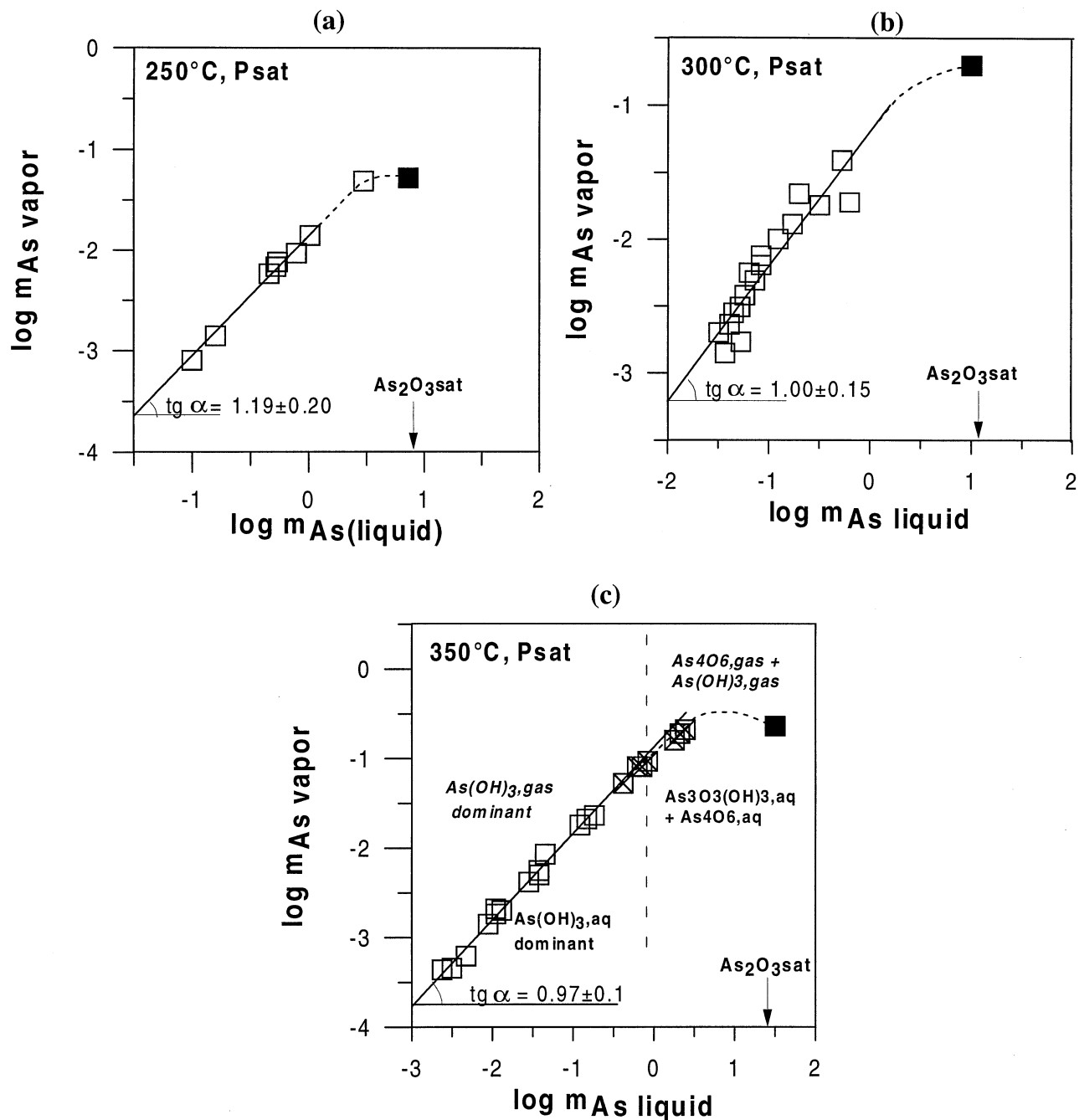
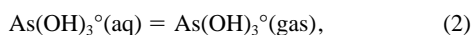


Fig. 5. As(III) vapor-phase vs. corresponding liquid-phase concentrations (log mol/kg of solution) measured in the system  $\text{As}_2\text{O}_3\text{-H}_2\text{O}$  at vapor-liquid equilibrium at 250, 300, and 350°C and  $P_{\text{sat}}$ . Open squares = experimental data obtained in this study for dilute and moderately concentrated arsenious acid solutions; straight solid lines = linear regression of these data points; closed symbols = data for the solutions saturated with respect to solid  $\text{As}_2\text{O}_3$  at each temperature. Dashed lines were drawn to aid the eye.

in the water vapor in equilibrium with these solutions according to the reaction



which is consistent with the slope (S)  $d \log m_{\text{As(gas)}}/d \log m_{\text{As(aq)}} = 1$ , where  $m$  is the corresponding As concentration. The formation in the vapor phase of other alternative monomer

species such as  $\text{HAsO}_2$  or  $\text{As(OH)}_3 \cdot n\text{H}_2\text{O}$ , also consistent with a slope of 1, can be excluded because neither changes in As coordination and distances in the first atomic shell ( $N_{\text{As-O}} = 3.0$ ;  $R_{\text{As-O}} = 1.78 \text{ \AA}$ ) nor second-shell water molecules were detected by our EXAFS measurements (see above) of supercritical fluids with densities close to those in the vapor phase (e.g., density  $\sim 0.1 \text{ g cm}^{-3}$  both at 350°C/ $P_{\text{sat}}$  and 500°C/250

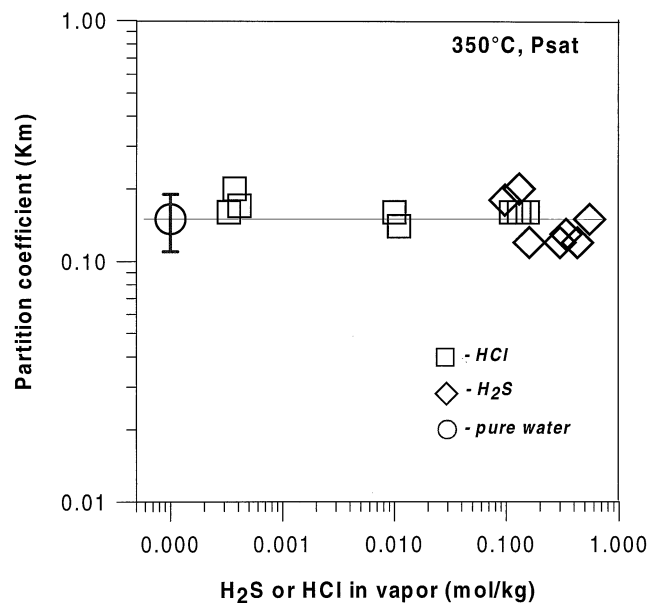


Fig. 6. As(III) vapor/liquid partition coefficient ( $K_m$ ) as a function of HCl or  $H_2S$  concentration in the vapor phase at  $350^\circ\text{C}$  and  $P_{\text{sat}}$ . The values of  $K_m$  in the presence of HCl and  $H_2S$  are the same as in pure water and independent of HCl or  $H_2S$  concentration. This demonstrates that As-chloride and As-sulfide complexes are negligible; and the  $\text{As}(\text{OH})_3$  dominates in the vapor phase at HCl and  $H_2S$  contents typical of hydrothermal fluids.

bar). No stable hydration shell around the  $\text{As}(\text{OH})_3$  molecule was also predicted, from thermodynamic considerations, in aqueous solution at these temperatures (Pokrovski et al., 1999). Molecular orbital calculations suggest that hydration can be neglected when estimating the energetics of As oxy-hydroxide neutral molecules in solution (Tossell, 1997). In the case of a pyramidal structure, the lone pair of electrons on the  $\text{As}(\text{OH})_3$  prevents close approach of the oxygen atom of water. Because the density of the saturated water vapor from 250 to  $350^\circ\text{C}$  is 100 to 5 times lower than that of the liquid water, the formation of a stable hydration shell around the neutral gaseous  $\text{As}(\text{OH})_3$  is unlikely. Although oxy-hydroxide species with reduced metal coordination such as  $\text{HBO}_2$  or  $\text{HAlO}_2$  have been reported at high temperature for other metals and metalloids like boron and aluminum (Chase et al., 1985), thermodynamic calculations demonstrate that their stabilities are extremely low at temperatures below  $800^\circ\text{C}$  and water pressures above 1 bar, in comparison to  $\text{B}(\text{OH})_3$  and  $\text{Al}(\text{OH})_3$ . As a result,  $\text{As}(\text{OH})_3(\text{gas})$  is likely to dominate As speciation in the vapor in equilibrium with dilute aqueous solutions up to the critical point of water, and in supercritical low-density fluids at temperatures to at least  $500^\circ\text{C}$ .

It can be seen in Figure 5 that at As liquid-phase concentrations higher than  $\sim 1\text{m}$ , there is a clear deviation from the linear relationship in the  $\log m_{\text{As}(\text{vapor})}$  vs.  $\log m_{\text{As}(\text{liquid})}$  plot, with a progressive decrease of the slope up to the point of solution saturation with  $\text{As}_2\text{O}_3$ . Recent Raman spectroscopy measurements (Gout et al., 1997) and ab initio calculations (Tossell, 1997) have shown that neutral cyclic oligomeric As oxy-hydroxide species such as  $\text{As}_3\text{O}_3(\text{OH})_3$ ,  $\text{As}_4\text{O}_6$ , and probably  $\text{As}_6\text{O}_6(\text{OH})_6$  form at the expense of the  $\text{As}(\text{OH})_3$  monomer in

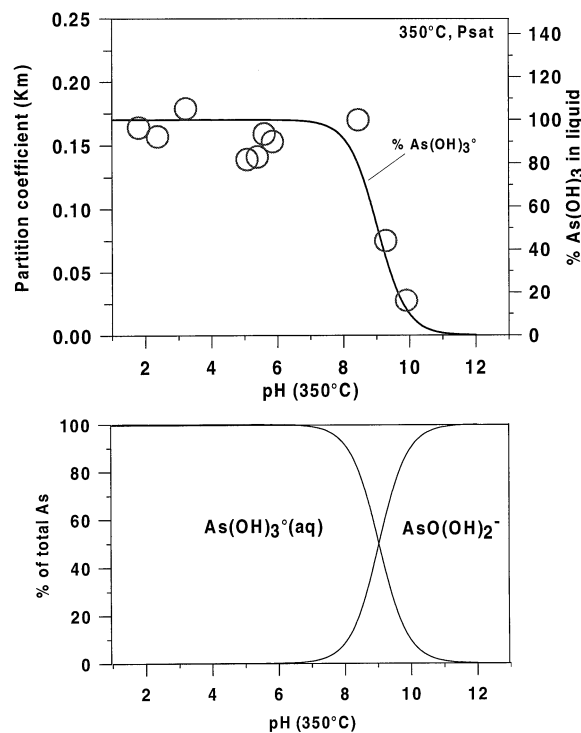


Fig. 7. As(III) vapor/liquid partition coefficient ( $K_m$ ) as a function of solution pH at  $350^\circ\text{C}$  and  $P_{\text{sat}}$  (upper graph). The symbols represent average values from experiments reported in Tables A1 to A3; the solid curve shows the percentage (with respect to total As) of the aqueous  $\text{As}(\text{OH})_3$  species in solution. The calculated distribution of As hydroxide species in solution as a function of pH at an ionic strength of 0.05 is shown in the lower graph. With increasing pH, the measured  $K_m$  values closely follow the amount of the neutral  $\text{As}(\text{OH})_3$  in solution, thus demonstrating that charged aqueous species ( $\text{AsO}(\text{OH})_2^-$ ) contribute insignificantly to the As volatility.

these concentrated solutions at temperatures above  $150^\circ\text{C}$ . The decrease of the slope can thus be explained by a significantly lower volatility of these heavier species in comparison to  $\text{As}(\text{OH})_3$ , and by a progressive decrease of the activity ( $\sim$ concentration) of the latter species in solution with increasing total aqueous As content. For example, for the reaction  $\text{As}_3\text{O}_3(\text{OH})_3(\text{aq}) + 3 \text{H}_2\text{O} = 3 \text{As}(\text{OH})_3(\text{gas})$ , and assuming that the activities of neutral species can be approximated by their corresponding concentrations,  $S$  should be equal to  $1/3$ . This is in agreement with  $S < 1$  observed at  $m_{\text{As}} \geq 1\text{m}$  at  $350^\circ\text{C}$  (Fig. 5c). More quantitative interpretation of the As vapor-phase solubilities in equilibrium with these concentrated solutions is, however, difficult because of the few data points obtained at concentrations above  $0.5\text{m}$  As as well as the absence of the stability constants for the As oligomeric aqueous complexes. Nevertheless, the results of our measurements clearly show that  $\text{As}(\text{OH})_3$  is the dominant As-bearing species in the vapor phase of the system  $\text{As}_2\text{O}_3\text{-H}_2\text{O}$  at  $P_{\text{sat}}$ .

Several liquid-vapor partitioning measurements were also performed at  $350^\circ\text{C}$  for arsenic acid ( $\text{H}_3\text{AsO}_4$ , Table A5). The obtained partition coefficients are independent, in the limit of their uncertainties, of  $\text{As}^{(\text{V})}$  aqueous concentration ranging from  $0.007$  to  $0.05\text{m}$ . The complex  $\text{AsO}(\text{OH})_3^-(\text{aq})$  is considered to be the dominant species in aqueous solution at the

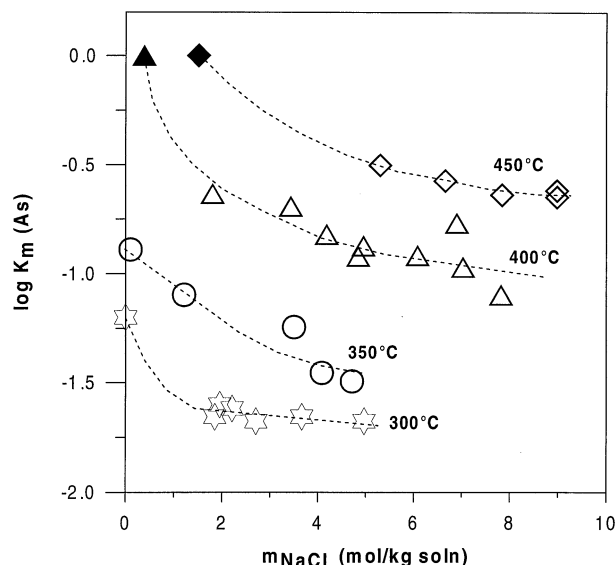


Fig. 8. As(III) vapor–liquid partition coefficients for H<sub>2</sub>O–NaCl solutions as a function of NaCl liquid concentration. Open symbols = experimental data points at indicated temperature; closed symbols =  $K_m = 1$  at the critical points of the NaCl–H<sub>2</sub>O system at 400 and 450°C. Dashed lines were drawn to aid the eye.

conditions of our experiments, as shown by thermodynamic calculations (Sergeeva and Khodakovsky, 1969; Baes and Mesmer, 1976) and recent XAFS spectroscopic measurements (Testemale et al., unpublished data). As a result, a species of the same stoichiometry forms in the vapor phase according to the equilibrium



The average  $K_m$  value for reaction 3 at 350°C reported in Table 2 indicates that arsenic acid is by a factor of 4 less volatile than its As(III) analog, arsenious acid.

### 3.2.2. H<sub>2</sub>O–HCl, H<sub>2</sub>O–H<sub>2</sub>S, and H<sub>2</sub>O–NaOH

Details on the measurements of As(III) vapor–liquid partition for dilute arsenious acid aqueous solutions in the presence of HCl or H<sub>2</sub>S at 350°C are reported in Table A2 of the Appendix. In Figure 6, the values of  $K_m$  (As) derived from these experiments are plotted as a function of HCl or H<sub>2</sub>S vapor-phase concentration. It can be seen that  $K_m$  values are identical to those in the pure-water system (section 3.2.1), and remain constant, in the limit of their uncertainties, up to at least 0.2m HCl and 0.5m H<sub>2</sub>S in the vapor phase. Previous solubility measurements (Pokrovski et al., 1996; Pokrovski et al., 2002a) and thermodynamic calculations (Heinrich and Eadington, 1986; Akinfiyev et al., 1992) indicate that sulfide and chloride As(III) complexes are negligible in near neutral H<sub>2</sub>S and moderately acid HCl solutions, respectively; and the hydroxide As(OH)<sub>3</sub> complex remains the dominant species. This result, together with the independence of  $K_m$  of H<sub>2</sub>S and HCl concentrations, indicates that As sulfide or chloride gaseous species should be insignificant, and the As(OH)<sub>3</sub> complex is dominant in the vapor phase in equilibrium with such solutions.

Measurements of As vapor–liquid partition for arsenious acid alkaline solutions at 350°C are reported in Table A3 of the Appendix. The corresponding  $K_m$  values are plotted in Figure 7 as a function of pH, together with those for H<sub>2</sub>O–HCl solutions discussed above. Because As(OH)<sub>3</sub><sup>o</sup>(aq) is known to

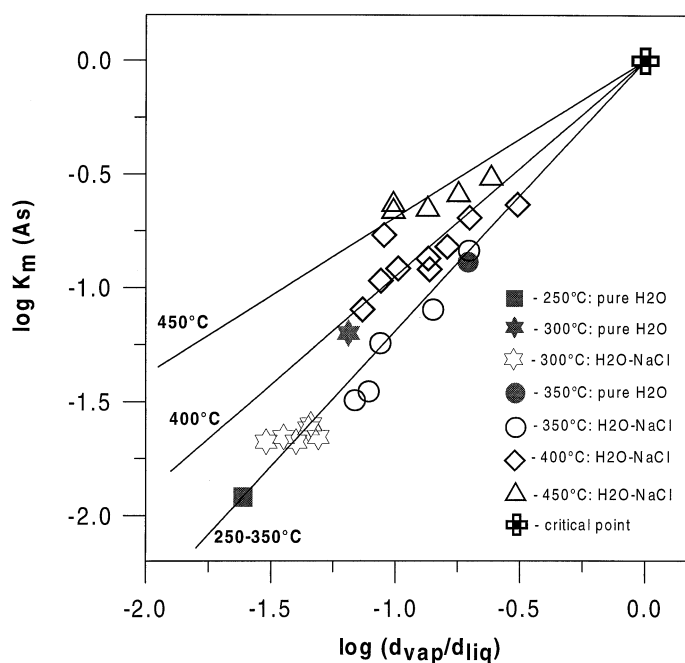


Fig. 9. Logarithm of As(III) vapor–liquid partition coefficient ( $K_m$ , Eqn. 1) as a function of the logarithm of vapor-to-liquid density ratio. Symbols = experimental data points at temperatures and compositions indicated in the figure; solid curves = regression of the data at 250 to 350; 400; and 450°C, according to Eqn. 4 (see text).

Table 3. Average As(III) concentrations in water-free vapor phase in equilibrium with crystalline or molten  $\text{As}_2\text{O}_3$  and the corresponding partial pressures of  $\text{As}_4\text{O}_6$  (ideal gas).

T (°C)	$C_{\text{As}}$ vapor (mol cm <sup>-3</sup> )	$\log_{10} P$ ( $\text{As}_4\text{O}_6$ , gas) (bar units $\pm 1\sigma$ )	Equilibrium phase	No. of runs
130	$1.14 \times 10^{-9}$	$-5.02 \pm 0.10$	Arsenolite	2
220	$1.70 \times 10^{-7}$	$-2.76 \pm 0.20$	Arsenolite	— <sup>a</sup>
250	$1.06 \times 10^{-6}$	$-1.94 \pm 0.15$	Arsenolite	4
265	$3.46 \times 10^{-6}$	$-1.41 \pm 0.11$	Arsenolite	1
300	$5.79 \times 10^{-6}$	$-1.16 \pm 0.10$	Arsenolite $\pm$ $\text{As}_2\text{O}_3$ melt	2
350	$1.07 \times 10^{-5}$	$-0.86 \pm 0.10$	$\text{As}_2\text{O}_3$ melt	2

<sup>a</sup> Extrapolated to zero water pressure from runs 20 and 4c at 220°C (see Table A7 of the Appendix).

dissociate in dilute basic solutions forming  $\text{AsO}(\text{OH})_2^-$  anion (Baes and Mesmer, 1976), the  $K_m$  values can be directly compared with the percentages of the neutral complex and its charged counterpart. To allow this comparison, solution pHs and As hydroxide species distribution were calculated at 350°C and  $P_{\text{sat}}$  (Table A3, Fig. 7). In these calculations, the dissociation constants for  $\text{H}_2\text{O}$ ,  $\text{HCl}$ , and  $\text{NaOH}$  were used from Sweeton et al. (1974), Tagirov et al. (1997), and Shock et al. (1997), respectively. The ionization constant for the reaction  $\text{As}(\text{OH})_3 = \text{AsO}(\text{OH})_2^- + \text{H}^+$  was predicted at 350°C by using Helgeson-Kirkham-Flowers (HKF) equation-of-state parameters on the bases of potentiometric measurements from 20 to 200°C of Pokrovski (1996) (Table 4). This value ( $\text{p}K_{350^\circ\text{C}} = 9.3 \pm 0.3$ ) is in good agreement with predictions of Smith et al. (1986) and Shock et al. (1997) ( $\text{p}K_{350^\circ\text{C}} = 9.0$  and  $9.2$ , respectively). It can be seen in Fig. 7 that the measured  $K_m$  values (symbols) decrease at pH above  $\sim 9$ . This decrease closely follows the percentage of the neutral  $\text{As}(\text{OH})_3$  species in solution (solid curve) predicted as a function of pH. This demonstrates again that the neutral  $\text{As}(\text{OH})_3$  complex forms in the vapor phase, and the charged complexes do not significantly contribute to As volatility. This is in agreement with the low dielectric constant of the vapor, which favors ion association and neutral complex stabilities (Pitzer and Pabalan, 1986; Brimhall and Crerar, 1987; Dandurand and Schott, 1992). Similar dependence on solution pH has been also found for the vapor–liquid partitioning of silicic and boric acids (Styrikovich et al., 1959; Martynova, 1964).

### 3.2.3. $\text{H}_2\text{O}$ -NaCl

Measurements of As(III) vapor–liquid partitioning at temperatures from 300 to 450°C and  $P_{\text{sat}}$  in the system  $\text{H}_2\text{O}$ -NaCl- $\text{As}_2\text{O}_3$  are reported in Table A4 of the Appendix. In Fig. 8,  $K_m$  values for As(III) in the presence of NaCl are plotted as a function of NaCl liquid-phase concentration. It can be seen in this figure that at 300 and 350°C, these values decrease with increasing NaCl solution content to the saturation with the solid salt, by a factor of 3 to 5 in comparison to pure water. At temperatures above the  $\text{H}_2\text{O}$  critical point (400 and 450°C), this decrease is slightly greater, by a factor of 5 to 10, in comparison to the theoretical  $K_m = 1$  at the critical point of the  $\text{H}_2\text{O}$ -NaCl isotherms at corresponding temperature. Arsenic vapor–liquid distribution in the  $\text{H}_2\text{O}$ -NaCl system can be described by reaction 2, as supported by the XAFS spectroscopy (section 3.1) and vapor–liquid partitioning in pure water (section 3.2.1). The decrease of As solubility in the vapor phase can

be explained by salting-in effects for the aqueous  $\text{As}(\text{OH})_3$ , which arise from its interactions with NaCl in the liquid. Quantitative treatment of the activity coefficients for the neutral  $\text{As}(\text{OH})_3$  species in high-temperature  $\text{H}_2\text{O}$ -NaCl solutions, using, for example, the Setchénow (1892) equation as a function of ionic strength (e.g., Walther, 1997), or the Born (1920) electrostatic approach that is based on the dielectric constant of the solvent (e.g., Walther and Schott, 1988; Dandurand and Schott, 1992), is, however, difficult because of the large uncertainties associated with the estimation of both ionic strengths and solvent dielectric constants for  $\text{H}_2\text{O}$ -NaCl solutions at temperatures above 350°C and pressures below 300 bar.

A more convenient and universal way to express vapor–liquid distribution is to apply a density approach initially proposed by Styrikovich et al. (1955), Styrikovich et al., (1960) for solutes weakly soluble in the steam below the critical point of water:

$$K_m = (d_{\text{vap}}/d_{\text{liq}})^n, \quad (4)$$

where  $d_{\text{vap}}$  and  $d_{\text{liq}}$  are the densities of the vapor and liquid phases, respectively, and  $n$  is an empirical number characteristic of the solute. In a logarithmic plot, vapor–liquid distribution coefficients should thus be linearly dependent of the vapor-to-liquid density ratio and come to the critical point of the solvent where the vapor and liquid densities are the same and  $K_m = 1$ . It has been demonstrated that this simple model was valid for a number of salts, weakly volatile compounds (boric and silicic acids) (Styrikovich et al., 1960; Smith et al., 1987), and gases (Ellis and Fyfe, 1957) over about 200°C below the critical point of water. It can be seen in Figure 9 that a plot of  $\log K_m$ , measured in this study both in pure water and  $\text{H}_2\text{O}$ -NaCl solutions, vs.  $\log(d_{\text{vap}}/d_{\text{liq}})$  at temperatures below the critical point of water, gives a straight line for a wide range of densities, with a slope  $n = 1.19 \pm 0.03$ , which is consistent with Eqn. 4. At 400 and 450°C, distinct relationships are observed for  $\text{H}_2\text{O}$ -NaCl solutions, with slopes of  $0.95 \pm 0.04$  and  $0.69 \pm 0.03$ , respectively. For consistency with Eqn. 4, the regressions shown in Figure 9 were performed by fixing  $\log K_m$  and  $\log(d_{\text{vap}}/d_{\text{liq}})$  to zero at the critical points of water and  $\text{H}_2\text{O}$ -NaCl solutions. The value of  $n$  obtained for  $\text{As}(\text{OH})_3$  in this study below the water critical point ( $n \sim 1.2$ ) is close to that derived from natural vapor–liquid partitioning of arsenic at the Geysers Geothermal Field ( $n \sim 1.6$  to  $1.7$ ; Smith et al., 1987). Analogous neutral hydroxide species, such as boric and silicic acids, were found to exhibit a similar range of  $n$  values (0.9 for  $\text{B}(\text{OH})_3$  and 1.9 for  $\text{Si}(\text{OH})_4$ ; Styrikovich et al., 1960).

Note that the values of  $n$  derived in this study for  $\text{As}(\text{OH})_3$  decrease with increasing temperature above the critical point of water. This reflects the increasing affinity of  $\text{As}(\text{OH})_3$  for the vapor phase at higher temperatures for same vapor-to-liquid density ratios. Thus, it can be expected that at temperatures higher than  $\sim 450^\circ\text{C}$ , arsenic would be enriched in the vapor phase in comparison to the corresponding dense  $\text{H}_2\text{O}$ -NaCl brine and thus exhibit values of  $K_m \geq 1$  and  $n \leq 0$ , typical of the liquid-vapor distribution behavior of gases (Ellis and Fyfe, 1957; Smith et al., 1987). It is, however, difficult to make quantitative predictions of As partition using this density approach at temperatures above  $500^\circ\text{C}$  because of the small set of data and the absence of a rigorous physical-chemical basis for the extrapolation of the values of  $n$  to higher temperatures. Consequently, for practical purposes, and to allow a direct comparison with natural data (see below), we adopted an empirical equation describing As(III) vapor-liquid partition in the system  $\text{H}_2\text{O}$ -NaCl as function of temperature and NaCl concentration:

$$\log K_m(\text{As}) = -0.0050 t^\circ \log m_{\text{NaCl}} + 1.385 \log m_{\text{NaCl}} \quad (5)$$

$$+ 0.012 t^\circ - 5.265,$$

where  $K_m$  stands for vapor-liquid partition coefficient for As (Eqn. 1),  $m_{\text{NaCl}}$  denotes NaCl liquid-phase concentration (in mol/kg of solution), and  $t^\circ$  is temperature ( $^\circ\text{C}$ ). Eqn. 5 reproduces the  $K_m(\text{As})$  values measured in this study at  $m_{\text{NaCl}} \geq 1$  m from 300 to  $450^\circ\text{C}$  in the limit of  $\pm 0.1 \log K_m$ . A regular dependence of  $\log K_m$  on temperature and NaCl concentration (Fig. 14) permits the use of this equation for extrapolation purposes at temperatures to at least  $600^\circ\text{C}$  with a confidence of about  $\pm 0.3 \log$  units.

### 3.3. $\text{As}_2\text{O}_3$ Vapor-Phase Solubility

Raw data on  $\text{As}_2\text{O}_3$  vapor-phase solubility measurements with and without  $\text{H}_2\text{O}(\text{gas})$  conducted by use of the ampoule and quenching techniques are reported, respectively, in Tables A6 and A7 of the Appendix. As it can be seen in Table A6, both in the water-free system and in the presence of water, steady-state As vapor-phase concentrations were attained after  $\sim 2$  d at  $250^\circ\text{C}$  and  $350^\circ\text{C}$ . Although no kinetic tests were conducted at other temperatures, a duration of 15 and 10 d, respectively, for the experiments at  $130^\circ\text{C}$  and 220, 265, and  $300^\circ\text{C}$  was considered to be enough to attain a steady state. A rapid attainment of equilibrium (within  $\sim 1$  h) between the vapor-phase and arsenolite in a dry system even at temperatures as low as  $100^\circ\text{C}$  has been demonstrated by previous works (Behrens and Rosenblatt, 1972, and references therein). Following these studies, and the satisfactory reproducibility of our measurements at similar pressures but different duration or in different experiments (Tables A6 and A7), As contents measured in the vapor phase at all temperatures were assumed to be in equilibrium with the solid (or molten) phase. The results obtained in the dry system and in the presence of  $\text{H}_2\text{O}$  are discussed below.

#### 3.3.1. Water-free system

Average As(III) concentrations in the water-free vapor phase in equilibrium with arsenolite or molten  $\text{As}_2\text{O}_3$  are reported in

Table 3. The solid phase after experiments at temperatures from 130 to  $250^\circ\text{C}$  remained unchanged, always corresponding to arsenolite. At  $350^\circ\text{C}$ , only amorphous  $\text{As}_2\text{O}_3$  was detected, indicating that all solid melted completely in these experiments. At  $300^\circ\text{C}$  and  $265^\circ\text{C}$ , arsenolite remained the dominant phase but exhibited traces of partial melting. As has been shown by previous spectroscopic (Ban and Knox, 1970; Beattie et al., 1970; Brumbach and Rosenblatt, 1972) and pressure or vaporization-rate measurements (Jungermann and Plieth, 1967; Behrens and Rosenblatt, 1972), the vapor in equilibrium with arsenic trioxide consists of  $\text{As}_4\text{O}_6$  molecules up to at least  $800^\circ\text{C}$ . Assuming an ideal behavior of  $\text{As}_4\text{O}_6$  in the vapor phase (Behrens and Rosenblatt, 1972), partial pressures of  $\text{As}_4\text{O}_6(\text{gas})$  in equilibrium with solid or molten  $\text{As}_2\text{O}_3$  can be calculated from the vapor As concentrations measured in this study:

$$P_{\text{As}_4\text{O}_6} = 0.25 C_{\text{As}} RT, \quad (6)$$

where  $C_{\text{As}}$  is the total As concentration in the vapor ( $\text{mol cm}^{-3}$ ), 0.25 is the conversion coefficient between As and  $\text{As}_4\text{O}_6$  molal concentrations,  $R$  is the ideal gas constant ( $R = 83.143 \text{ bar cm}^3 \text{ mol}^{-1} \text{ K}^{-1}$ ),  $T$  is temperature (K), and  $P$  is  $\text{As}_4\text{O}_6$  pressure (bar). The values of  $\log_{10}(P_{\text{As}_4\text{O}_6})$  derived in this study by Eqn. 6 are reported in Table 3 and compared with the data reported in the literature in Figure 10. Despite the small number of experiments performed in a dry system in the present study, our  $\text{As}_4\text{O}_6$  pressures are in good agreement (in the limit of  $\pm 0.1 \log P$ ) with the many data reported in the literature that were obtained from direct  $P_{\text{As}_4\text{O}_6}$  measurements in equilibrium with arsenolite up to  $300^\circ\text{C}$ . The pressure of  $\text{As}_4\text{O}_6$  above molten  $\text{As}_2\text{O}_3$  derived in our study at  $350^\circ\text{C}$  is also in reasonable agreement with the corresponding value reported by Rushton and Daniels (1926) from direct measurements. At 300 and  $265^\circ\text{C}$ ,  $\text{As}_4\text{O}_6$  vapor pressures of the present study are close to those obtained by extrapolation of the Rushton and Daniels (1926) curve for molten  $\text{As}_2\text{O}_3$  to lower temperatures. Because the melting temperature of arsenolite is  $\sim 275^\circ\text{C}$ , the  $\text{As}_4\text{O}_6$  pressures at 265 and  $300^\circ\text{C}$  from the present study can be explained by the presence of a melt in our experiments (Rushton and Daniels, 1926; Schulman and Schumb, 1943), which is also in agreement with our observations of the solid phases after the runs (see above).

#### 3.3.2. $\text{As}_2\text{O}_3$ - $\text{H}_2\text{O}$

Arsenic (III) vapor-phase concentrations measured in the presence of  $\text{H}_2\text{O}(\text{gas})$  are plotted in Figure 11 as a function of water vapor pressure. The solid phase after experiments below  $265^\circ\text{C}$  was dominated by arsenolite as showed X-ray diffraction and Raman spectroscopy. However, optical observations and weight-loss controls demonstrated the presence of an amorphous hydrated  $\text{As}_2\text{O}_3$  phase ( $< \sim 10$  to 50 wt% of the total solid) whose quantity generally increased with increasing temperature. At  $300^\circ\text{C}$ , this amorphous phase dominated in the solid products after experiments. Because of its important amounts, the formation of such a phase cannot be explained by the condensation of vapor-dissolved arsenic trioxide during quenching, which could represent no more than 5 wt% of the total solid. Although claudetite (monoclinic  $\text{As}_2\text{O}_3$ ) is considered to be the thermodynamically stable phase at temperatures

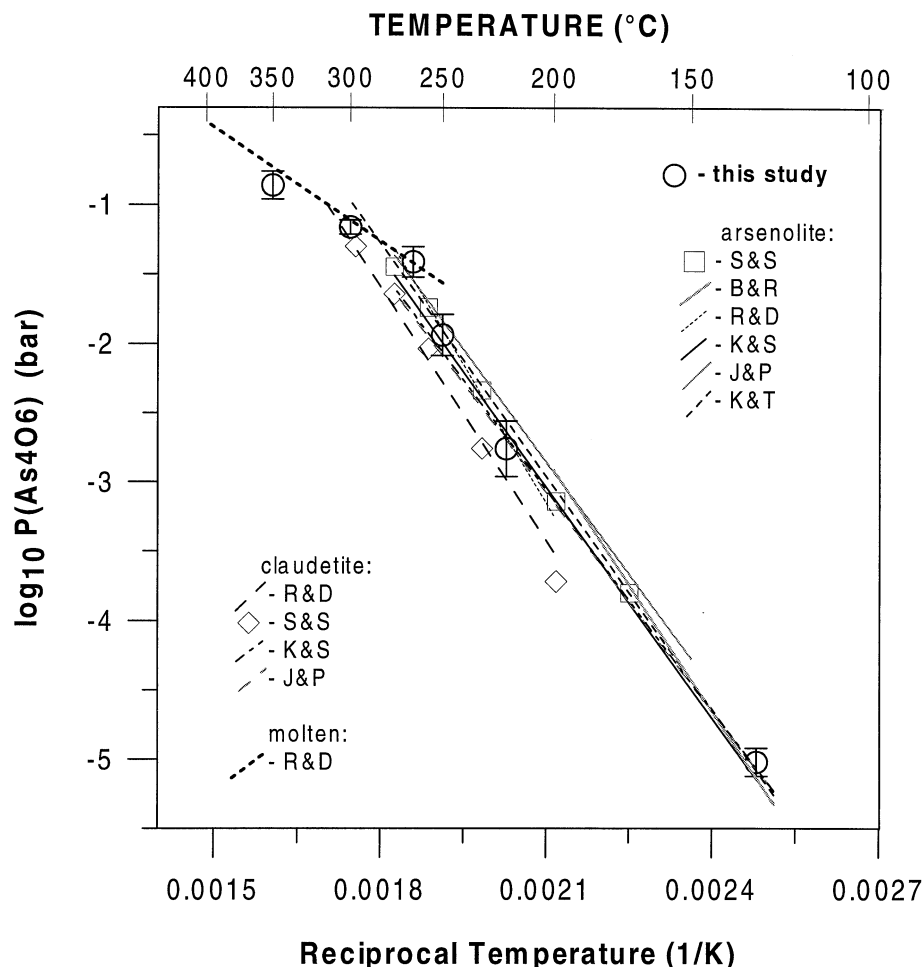


Fig. 10. Logarithm of the pressure of  $\text{As}_4\text{O}_6$  (gas) in a water-free system in equilibrium with cubic (arsenolite), monoclinic (claudetite), or molten arsenic trioxide ( $\text{As}_2\text{O}_3$ ) as a function of reciprocal temperature. The symbols and curves stand for experimental data derived from this study and are taken from the references indicated in the figure: B&R, Behrens and Rosenblatt (1972); J&P, Jungermann and Plieth (1967); K&S, Karutz and Stranski (1957); K&T, Kazenas and Tsvetkov (1997); R&D, Rushton and Daniels (1926); S&S, Schulman and Schumb (1943).

to 300°C, thus having lower vapor pressures than arsenolite (Fig. 10; Rushton and Daniels, 1926; Schulman and Schumb, 1943), this phase was never detected after our experiments. Nevertheless, initial stages of the arsenolite-to-claudetite transformation in the presence of water cannot be excluded in our experiments. Indeed, previous studies have demonstrated claudetite formation from arsenolite between 150 and 300°C in the presence of water (Schulman and Schumb, 1943; Chang and Bestul, 1971; Pokrovski et al., 1996). It should be noted that the arsenolite-to-claudetite solid-phase transition requires important structural rearrangements, which consist in a complete breakage of the arsenolite cubic structure composed of  $\text{As}_4\text{O}_6$  molecules, followed by the formation of two-dimensional networks composed of As-O-As-O chains, typical of claudetite structure (Chang and Bestul, 1971). Because of such significant structural changes, this transformation should pass through an intermediate glassy state (Rushton and Daniels, 1926; Chang and Bestul, 1971). Such a metastable phase is likely to be observed in our experiments below and at 300°C in the presence of water.

It can be seen in Figure 11 that at low  $\text{H}_2\text{O}$  pressures, As vapor solubilities measured at 130 and 265°C decrease by  $\sim 1.5$  to 2 times in comparison to the water-free system. If As speciation in the vapor is dominated by the anhydrous  $\text{As}_4\text{O}_6$  species (section 3.3.1) and the equilibrium solid phase remained unchanged, As vapor-phase solubility would be independent of water pressure. Consequently, the observed decrease is most likely due to the formation of an intermediate glassy or claudetite-like phase, whose volatility is lower than that of arsenolite. At higher water pressures, As concentrations in the vapor remain about the same at 250 and 265°C, but increase at 220°C (Fig. 11). This can be interpreted by the formation in the vapor of hydrated As species whose concentration compensates the decrease of  $\text{As}_4\text{O}_6$  vapor content ( $\sim$ partial pressure) due to the phase transformation. Following the results on vapor-liquid partition for concentrated solutions (section 3.2.1), it is suggested that  $\text{As}(\text{OH})_3$  could form in significant amounts at  $\text{H}_2\text{O}$  pressures close to the saturation. At 300°C, the possible solubility increase due to hydration is likely to be completely masked by arsenolite melting (see above).

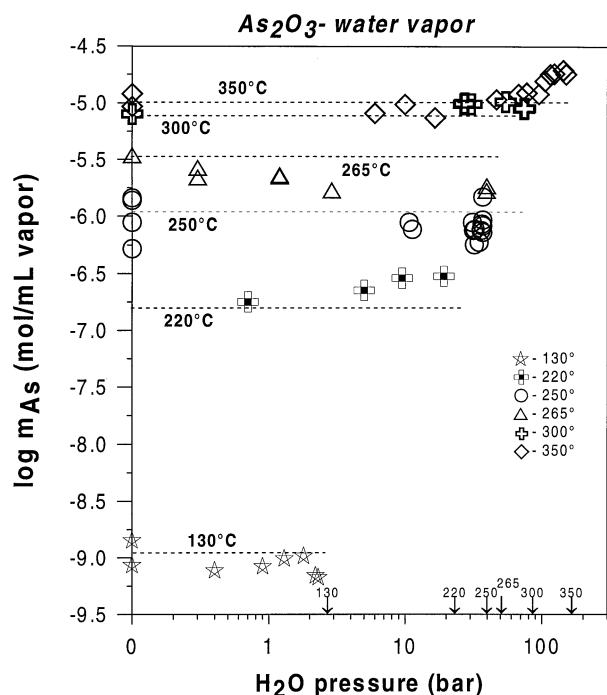


Fig. 11. Arsenic vapor-phase concentrations (expressed in mol As/mL of vapor, in  $\log_{10}$  units), as a function of water vapor pressure, in equilibrium with arsenic trioxide. Symbols = data measured in this study at stated temperatures; arrows = saturated pressure of pure water at each indicated temperature; horizontal dashed lines = concentration of  $\text{As}_4\text{O}_6(\text{gas})$  species measured in this study in a dry system in equilibrium with arsenolite (130 to 300°C) or molten  $\text{As}_2\text{O}_3$  (350°C), and assuming an ideal gas behavior for  $\text{As}_4\text{O}_6$  (Table 3 and text).

At 350°C, no arsenolite was detected after experiment, and the  $\text{As}_2\text{O}_3$  glass contained significant amounts of water (~5 to 10 wt%), as inferred from weight-loss control. Moreover,  $\text{H}_2\text{O}$  pressure monitored in the 350°C experiments was found to be lower than that calculated from the quantity of water loaded in the reactor before experiment. This difference can be explained by the dissolution of  $\text{H}_2\text{O}(\text{gas})$  in the molten  $\text{As}_2\text{O}_3$ , and was found to attain 10 wt% (~0.9 in mole fraction) in experiments carried out at water pressures higher than 100 bar. It can be seen in Figure 11 that As vapor-phase solubility clearly increases with increasing pressure at  $P_{\text{H}_2\text{O}} \geq \sim 40$  bar. The Pointing correction (which accounts for the increase in the fugacity of the molten  $\text{As}_2\text{O}_3$  at pressures higher than the vapor pressure of the melt itself; Sandler, 1985) was found to not exceed 15% of the total vapor solubility at the highest pressure measured (150 bar). As a result, this solubility increase clearly demonstrates the formation, in the 350°C experiments, of hydrolyzed/hydrated arsenic species other than  $\text{As}_4\text{O}_6$ . The exact quantification of species stoichiometry and stability from these experiments is, however, impossible because of the expected continued changes in the melt properties due to  $\text{H}_2\text{O}$  dissolution with increasing  $\text{H}_2\text{O}$  pressure. A very rough estimation of the hydrated species contribution to the solubility at 350°C could be performed assuming an ideal  $\text{H}_2\text{O}-\text{As}_2\text{O}_3$  solution in the melt ( $\text{As}_4\text{O}_6$  mole fraction ~0.1 to 0.2 at  $P > 100$  bar), which implies that at the highest pressure investigated (150 bar), As hydrolyzed species should account for ~90% of the

total As in the vapor phase. These crude estimations are, nevertheless, in reasonable agreement with the stability of  $\text{As}(\text{OH})_3(\text{gas})$  species derived below.

#### 4. CHARACTERIZATION OF THE THERMODYNAMIC PROPERTIES OF GASEOUS ARSENIC OXY-HYDROXIDE SPECIES

##### 4.1. Conventions, Units, and Standard States

The Gibbs free energies (and enthalpies) of minerals, gases, and aqueous species are represented in this study as apparent standard molal Gibbs free energies ( $\Delta G^\circ_{P,T}$ ) (and enthalpies,  $\Delta H^\circ_{P,T}$ ) of formation from the elements at the subscripted pressure (P) and temperature (T) (Shock et al., 1997):

$$\Delta G^\circ_{P,T} = \Delta_f G^\circ + (G^\circ_{P,T} - G^\circ_{Pr,T_r}), \quad (7)$$

where  $\Delta_f G^\circ$  is the standard molal Gibbs free energy of formation of the species from its elements in their stable state at the reference pressure ( $P_r = 1$  bar) and temperature ( $T_r = 298.15$  K), and  $(G^\circ_{P,T} - G^\circ_{Pr,T_r})$  refer to differences in the standard molal Gibbs free energy of the species that arise from changes in pressure ( $P-P_r$ ) and temperature ( $T-T_r$ ). The reference states for the elements (for which  $\Delta G^\circ_{1,298}$  (and  $\Delta H^\circ_{1,298}$ ) = 0) in the system As-O-H are native arsenic (As, rhombohedral);  $\text{O}_2$ , ideal gas; and  $\text{H}_2$ , ideal gas. The standard states for the solid phases and  $\text{H}_2\text{O}$  are unit activity for the pure phase at all temperatures and pressures. The standard state for gaseous species is characterized by unit fugacity of the ideal gas at 1 bar and any temperature. For aqueous species, the reference state convention corresponds to unit activity coefficient for a hypothetical one molal solution whose behavior is ideal. At low to moderate solution ionic strengths ( $\leq \sim 0.1$ ), activity coefficients of neutral aqueous species were assumed to be unity, but those of charged species were calculated by the extended Debye-Hückel equation (Garrels and Christ, 1965).

##### 4.2. Henry Constants for $\text{As}(\text{OH})_3$ and $\text{AsO}(\text{OH})_3$ Vapor-Liquid Equilibria

The data on vapor-liquid partitioning in pure water at  $P_{\text{sat}}$  for  $\text{As}(\text{OH})_3$  at 250, 300, and 350°C allow determination of the thermodynamic properties of  $\text{As}(\text{OH})_3(\text{gas})$  by using the corresponding properties of  $\text{As}(\text{OH})_3(\text{aq})$  and the conventional Henry constant ( $K_h$ , Naumov et al., 1974) for vapor-liquid equilibrium for reaction 2:

$$K_h = f_{\text{As}(\text{OH})_3(\text{gas})} / a_{\text{As}(\text{OH})_3(\text{aq})}, \quad (8)$$

where  $f$  and  $a$  stand, respectively, for the vapor-phase fugacity and aqueous-phase activity of the subscripted species. According to the convention (section 4.1), the activity of  $\text{As}(\text{OH})_3(\text{aq})$  in pure water can be replaced by its corresponding molality. Following the low As vapor-phase concentrations, and assuming the absence of significant  $\text{As}(\text{OH})_3-\text{H}_2\text{O}$  interactions in the low-density vapor phase in our experiments ( $\leq 0.1 \text{ g cm}^{-3}$ ),  $\text{As}(\text{OH})_3(\text{gas})$  fugacity can be approximated by its partial pressure defined as

$$f_{\text{As}(\text{OH})_3(\text{gas})} \approx P_{\text{As}(\text{OH})_3(\text{gas})} = P_{\text{tot}} X_{\text{As}}, \quad (9)$$

where  $P_{\text{tot}}$  is the total pressure in the system ( $\approx P_{\text{H}_2\text{O}}$ ), and  $X_{\text{As}}$

Table 4. Standard molal thermodynamic properties of As(III) oxide and hydroxide gaseous and aqueous species at 25°C and 1 bar used or derived in this study.

Species	$\Delta_f G^\circ_{298}$ kJ/mol	$S^\circ_{298}$ J/mol K	$C_p^\circ_{298}$ J/mol K	$C_p$ equation (J/mol K) (temperature interval in K)	Reference
Gaseous species					
As <sub>4</sub> O <sub>6</sub> (gas)	-1092.3 ± 3.0	409.24 ± 10.50	173.6 ± 5.0	212.81 + 0.0186 T - 39.78 × 10 <sup>5</sup> T <sup>-2</sup> (298–1200)	Pankratz (1982)
As(OH) <sub>3</sub> (gas)	-575.5 ± 10.0 <sup>a</sup>	428.0 ± 30 <sup>a</sup>	84.5 ± 10.0 <sup>b</sup>	219.0 - 3.444 × 10 <sup>-3</sup> + 1.8708 × 10 <sup>6</sup> T <sup>-2</sup> 2667.6 T <sup>-0.5</sup> (298–1200) <sup>c</sup>	This study
Aqueous species					
HKF parameters (joule units)					
As(OH) <sub>3</sub> (aq)	-639.8 ± 0.5	200.0 ± 10.0	196.6 ± 25.0	a <sub>1</sub> × 10 = 35.44; a <sub>2</sub> × 10 <sup>-2</sup> = 53.97; a <sub>3</sub> = 2.85; a <sub>4</sub> × 10 <sup>-4</sup> = -13.85; c <sub>1</sub> = 209.2; c <sub>2</sub> × 10 <sup>-4</sup> = -6.28; ω = 0	Pokrovski et al. (1996)
AsO(OH) <sub>2</sub> <sup>-</sup>	-586.6 ± 0.9	117.2 ± 15.0	62.8 ± 30.0	a <sub>1</sub> × 10 = 25.44; a <sub>2</sub> × 10 <sup>-2</sup> = 29.54; a <sub>3</sub> = 12.43; a <sub>4</sub> × 10 <sup>-4</sup> = -12.84; c <sub>1</sub> = 108.11; c <sub>2</sub> × 10 <sup>-4</sup> = 0.084; ω × 10 <sup>-5</sup> = 4.98	Pokrovski (1996)

<sup>a</sup> From fitting As(OH)<sub>3</sub>(gas) Gibbs free energies at 250, 300, and 350°C (Table 2) using Eqn. 13.

<sup>b</sup> From correlation between C<sub>p</sub> of metallic fluoride and hydroxide gaseous species (Eqn. 11).

<sup>c</sup> By analogy with the heat capacity dependence of B(OH)<sub>3</sub>(gas) on temperature (Chase et al., 1985).

is the gas-phase mole fraction of As(OH)<sub>3</sub>. Note that such an approximation has been shown to be valid for H<sub>2</sub>O-gas mixtures at densities lower than 0.3 g cm<sup>-3</sup> (Garrels and Christ, 1965) and was also applied for interpreting the solubilities of low-volatile solids in water vapor (Alekhin and Vakulenko, 1988; Migdisov et al., 1999; Archibald et al., 2001). The Henry constant of reaction 2 can be thus calculated from the measured K<sub>m</sub> (Eqn. 1) as follows:

$$K_h = K_m P_{\text{H}_2\text{O}} / 55.51. \quad (10)$$

The values of K<sub>h</sub> derived at 250, 300, and 350°C for reaction 2 and at 350°C for reaction 3 are reported in Table 2. These data allow calculation of the Gibbs free energies of As(OH)<sub>3</sub>(gas) and AsO(OH)<sub>3</sub>(gas) (Table 2), provided that the corresponding properties of their aqueous counterparts at each experimental temperature are known. The free energies of aqueous arsenious acid, As(OH)<sub>3</sub>(aq), are at present relatively well constrained on the bases of solubility measurements to 300°C; and they can be extrapolated with confidence to higher temperatures by using the HKF equation of state (Table 4; Pokrovski et al., 1996). By contrast, the high-temperature thermodynamic properties of aqueous arsenic acid, AsO(OH)<sub>3</sub>(aq), are poorly known, and all existing predictions are based on scarce data at ambient temperature (e.g., Naumov et al., 1974; Shock et al., 1997). Consequently, the following discussion is devoted only to the As(OH)<sub>3</sub>(gas) thermodynamics.

### 4.3. Thermodynamic Properties of As(OH)<sub>3</sub>(gas)

The Gibbs free energies of As(OH)<sub>3</sub>(gas) reported in Table 2 at three experimental temperatures allow extrapolation to 25°C to derive the standard thermodynamic properties for this species. Such an extrapolation requires knowledge of the species

heat capacity as a function of temperature. These values could be generated with precision by using statistical thermodynamic approaches for ideal gas molecules provided that their geometry and all vibrational and rotational frequencies are exactly known (Lewis and Randall, 1965). Because of the lack of such information for As(OH)<sub>3</sub>(gas), in the present study, we decided to use well-known analogies between heat capacities of gaseous metallic (oxy-)hydroxide and fluoride species to derive the corresponding property for As(OH)<sub>3</sub>(gas). In Figure 12, the heat capacities of gaseous metal fluorides at 25°C are plotted vs. the corresponding values for analogous hydroxides of the same metals. The data presented in this figure were taken from the Joint Army-Navy-Air Force (JANAF) database (Chase et al., 1985). A good linear dependence (squared correlation coefficient = 0.98) is apparent in this figure, and described by

$$C_p^\circ(\text{OH}) = 1.10 C_p^\circ(\text{F}) + 12.22 \text{ (J/mol K)} \quad (11)$$

where C<sub>p</sub><sup>°</sup>(OH) and C<sub>p</sub><sup>°</sup>(F) stand for the standard molal isobaric heat capacity at 25°C of a metal hydroxide and its analogous fluoride species, respectively. Eqn. 11 allows determination of C<sub>p</sub><sup>°</sup>As(OH)<sub>3</sub>(gas) by using the corresponding value for AsF<sub>3</sub>(gas) (Naumov et al., 1974): C<sub>p</sub><sup>°</sup>As(OH)<sub>3</sub>(gas) = 84.5 ± 10.0 J/mol K. At temperatures above 25°C, the heat capacity of As(OH)<sub>3</sub>(gas) was approximated by an analogy with the chemically similar B(OH)<sub>3</sub>(gas) for which accurate C<sub>p</sub> values are available to at least 2000°C (Chase et al., 1985). Such an analogy is believed to be reliable because the temperature coefficients of heat capacities for ideal gas metallic species of similar stoichiometries depend only weakly on the metal atom itself, as demonstrated by statistical thermodynamics (e.g., Lewis and Randall, 1965; Chase et al., 1985). Thus, the C<sub>p</sub> B(OH)<sub>3</sub> values tabulated in Chase et al. (1985) were fitted from

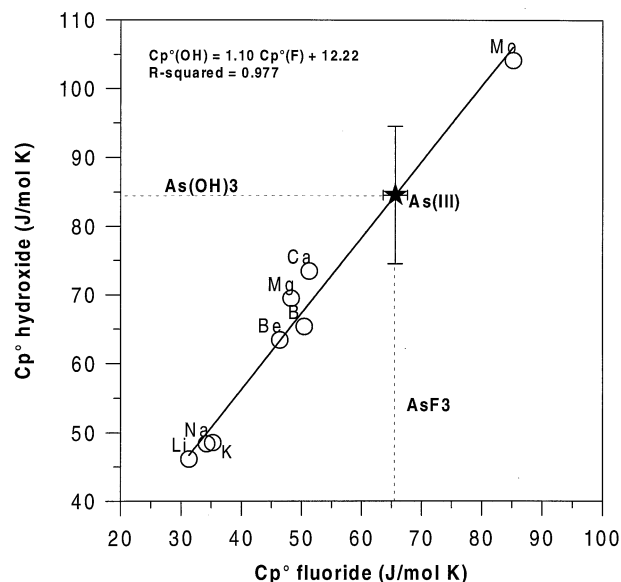


Fig. 12. Correlation between standard molal isobaric heat capacities at 25°C, 1 bar, for gaseous hydroxide and fluoride species of metals and metalloids. Circles = fluoride–hydroxide pairs for metals indicated in the figure (LiF–LiOH, NaF–NaOH, KF–KOH, BeF<sub>2</sub>–Be(OH)<sub>2</sub>, MgF<sub>2</sub>–Mg(OH)<sub>2</sub>, CaF<sub>2</sub>–Ca(OH)<sub>2</sub>, BF<sub>3</sub>–B(OH)<sub>3</sub>, MoF<sub>4</sub>–MoO<sub>2</sub>(OH)<sub>2</sub>; data from Chase et al., 1985); solid line = linear regression of these data. The heat capacity of As(OH)<sub>3</sub> (star) was determined by using this correlation and the corresponding value for AsF<sub>3</sub> (from Naumov et al., 1974).

298 to 2000 K by using an extended Maier-Kelley equation in the form  $C_p(T) = A + B \times T + C \times T^{-2} + D \times T^{-0.5}$ , where  $T$  is temperature (K) and  $A$ ,  $B$ ,  $C$ , and  $D$  are regression coefficients (Maier and Kelley, 1932). This equation reproduces the gaseous boric acid heat capacities in the limit of 0.2 J/mol K in the temperature range 25 to ~2000°C. The obtained  $B$ ,  $C$ , and  $D$  coefficients, which reflect the temperature dependence of  $C_p$ , were kept the same for As(OH)<sub>3</sub>(gas), but coefficient  $A$  was adjusted to match the value of 84.5 J/mol K for  $C_p$  As(OH)<sub>3</sub>(aq) at 25°C, derived by Eqn. 11:

$$C_p^\circ(\text{As(OH)}_3, \text{gas}) = 219.0(\pm 10) - (3.444 \pm 0.23) \times 10^{-3} T + (1.8708 \pm 0.04) \times 10^6 T^{-2} - (2667.6 \pm 22) T^{-0.5}. \quad (12)$$

Then, the Gibbs free energies of As(OH)<sub>3</sub>(gas) at 250, 300, and 350°C (Table 2) were fitted by the equation

$$\Delta G_{p,T} = \Delta_f G_{1,298}^\circ - S_{1,298}^\circ(T - 298.15) + \int_{298.15}^T C_p(T) dT - T \int_{298.15}^T \frac{C_p(T)}{T^2} dT \quad (13)$$

where  $T$  is absolute temperature (K);  $\Delta_f G_{1,298}^\circ$  and  $S_{1,298}^\circ$  are fitting coefficients and refer to the standard molal Gibbs free energy and entropy of As(OH)<sub>3</sub>(gas) at 25°C and 1 bar; and  $\int$  represent an integral from 298.15 to  $T$  of the heat capacity function defined by Eqn. 12. The obtained values of  $\Delta_f G_{1,298}^\circ$  and  $S_{1,298}^\circ$  are  $-575.5 \pm 10.0$  kJ/mol and  $428 \pm 30$  J/mol K, respectively. The uncertainties on these values stem from those associated with the Gibbs free energies at each experimental

temperature (Table 2), Eqn. 12 coefficients, and Eqn. 13 fitting. The thermodynamic parameters of As(III) (oxy-)hydroxide gaseous and aqueous complexes used or derived in this study are summarized in Table 4. In Figure 13, the values of  $\log K_h(2)$  measured in this study (symbols) and calculated by using the parameters from Table 4 (solid line) are plotted vs. reciprocal temperature. They are compared with the values generated by using the “density model” by combining Eqn. 4 and 10 (dashed line). It can be seen that the density model can be used to predict As(III) vapor–liquid fractionation at temperatures above ~170°C. At lower temperatures, however, such a simple model should be used with caution because of large differences with the more rigorous thermodynamic approaches (Eqn. 13).

#### 4.4. Arsenic (III) Gaseous Speciation in the System As<sub>2</sub>O<sub>3</sub>–H<sub>2</sub>O

Combining As(OH)<sub>3</sub> standard Gibbs free energies calculated as a function of temperature by using the parameters reported in Table 4, with the corresponding values for As<sub>4</sub>O<sub>6</sub>(gas), one can estimate the relative stabilities of these two main As(III) gaseous species in the system As<sub>2</sub>O<sub>3</sub>(solid/melt)–H<sub>2</sub>O(gas). To perform these calculations, the thermodynamic properties for As<sub>4</sub>O<sub>6</sub>(gas) were adopted from Pankratz (1982) (Table 4). This accurate set of data is based on arsenolite vapor pressure measurements and statistical thermodynamics calculations (Behrens and Rosenblatt, 1972), and it is in good agreement with the As<sub>2</sub>O<sub>3</sub> vapor-phase solubilities in a water-free system obtained in this study (section 3.3).

Calculations show that As(OH)<sub>3</sub>(gas) accounts for 40 to 60% of the total As in the vapor phase in equilibrium with As<sub>2</sub>O<sub>3</sub> at temperatures from 130 to 300°C and H<sub>2</sub>O pressures close to the saturation. This should correspond to a solubility increase by a factor of two in comparison to the water-free system provided that the equilibrium solid phase remains unchanged. Although within the range of the experimental uncertainties for the measured As<sub>2</sub>O<sub>3</sub> solubilities below 300°C (Tables A6 and A7, Fig. 11), this potential increase is masked by the “arsenolite-to-glass” transition inferred in our experiments in the presence of water. Such a transition should lower As<sub>4</sub>O<sub>6</sub>(gas) concentration by ~2 times in comparison to the water-free system (section 3.3). Therefore, the decrease of As<sub>4</sub>O<sub>6</sub> concentration with increasing water pressure can be compensated by the increase of As(OH)<sub>3</sub>, so that the total As vapor concentration remains about constant in the limit of ±50% of the value (section 3.3).

At 350°C, calculations indicate that As(OH)<sub>3</sub>(gas) would account for 90% of the total As in the vapor phase at pressures above 150 bar. This is also in reasonable agreement with the observed water dissolution in the molten As<sub>2</sub>O<sub>3</sub>, which should lower significantly the As<sub>2</sub>O<sub>3</sub> activity in the melt, and, consequently, the As<sub>4</sub>O<sub>6</sub> concentration in the vapor phase in comparison to the dry system, so that the resulting total As vapor concentrations measured in these experiments increase by only a factor of 2 to 3 at water pressures close to  $P_{\text{sat}}$  (section 3.3, Fig. 11).

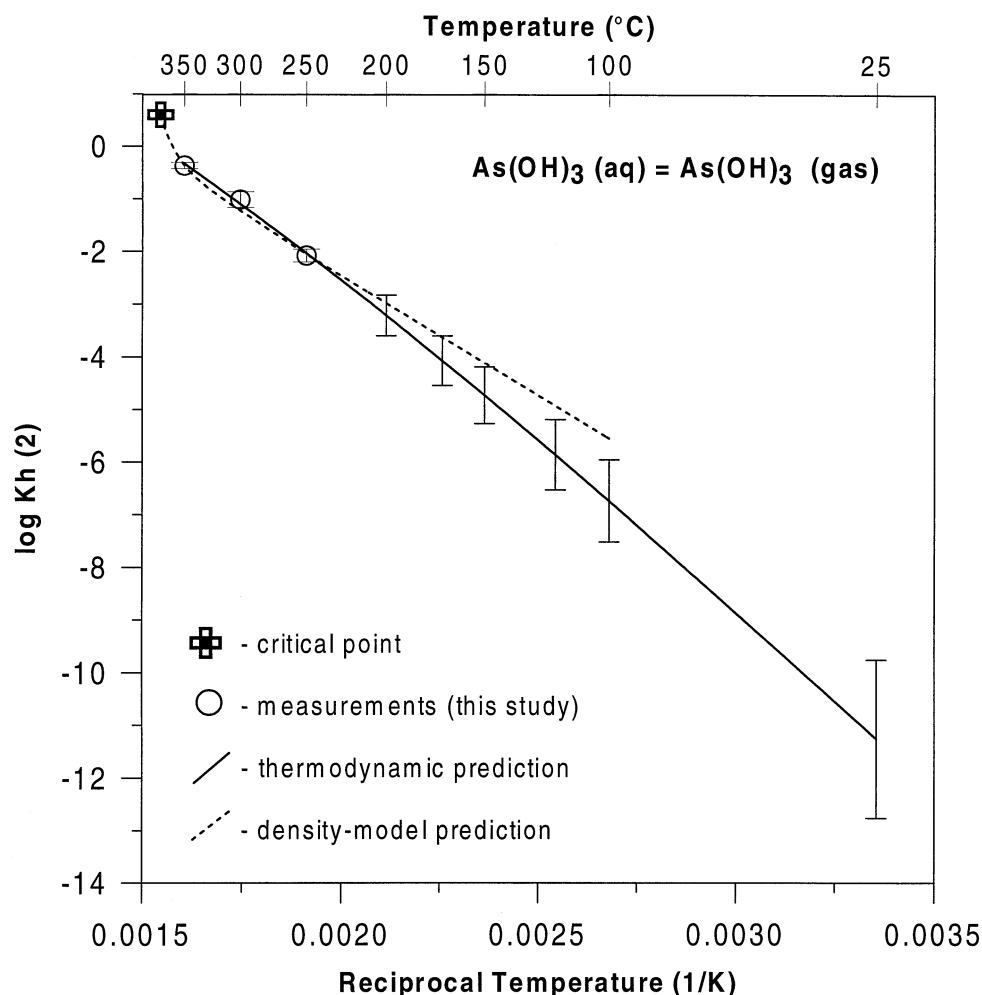


Fig. 13. Plot of the logarithm of the Henry constant for reaction 2 vs. the reciprocal of absolute temperature. Circles = experimental data obtained in this study; solid line = fit through this data by using Eqns. 12 and 13. The error bars on this curve correspond to fit uncertainties (at 95% probability level). The dashed curve was calculated from the density model according to Eqn. 4 (see text for details).

## 5. INTERPRETATION OF As VAPOR-LIQUID FRACTIONATION IN HYDROTHERMAL FLUIDS AND As TRANSPORT IN VOLCANIC GASES

### 5.1. Boiling Hydrothermal Systems

The results of this study demonstrate that  $\text{As(OH)}_3(\text{gas})$  is by far the most dominant arsenic species in the vapor phase produced through boiling of hydrothermal fluids. In spite of the known enrichment of the vapor, in comparison to the liquid, in volatile species such as HCl and  $\text{H}_2\text{S}$  during boiling (Drummond and Ohmoto, 1985; Bowers, 1990), our experiments suggest that nevertheless As chloride and sulfide gaseous complexes are negligible at the HCl and  $\text{H}_2\text{S}$  concentrations typically found in the steams of modern hydrothermal fields and fluid inclusions in minerals from hydrothermal-magmatic ore deposits (Ballantyne and Moore, 1988; Hedenquist and Lowenstern, 1994; Heinrich et al., 1999). The vapor-liquid partition coefficients for  $\text{AsO(OH)}_3(\text{gas})$  derived in this study, combined with the thermodynamic properties of As(V) oxy-hydroxide aqueous species and minerals (Naumov et al., 1974; Shock et

al., 1997), suggest that As(V) species are not stable in natural reducing hydrothermal environments. Thus, the  $\text{As(OH)}_3$  partition coefficients measured in the present work can be directly compared with As vapor-liquid fractionations observed in natural hydrothermal boiling fluids. In Figure 14, we plotted arsenic vapor-liquid distribution coefficients (defined by Eqn. 1) measured in steam-water discharges of modern hydrothermal systems, and in coexisting vapor and brine fluid inclusions in quartz from magmatic-hydrothermal deposits. It can be seen in this figure that at temperatures below  $300^\circ\text{C}$ , As concentrations in steam from modern geothermal systems (e.g., Geysers, Otake, Cerro Prieto, see Ballantyne and Moore, 1988) are generally 2 to 3 orders of magnitude lower than those in the low-salinity liquid phase ( $< \sim 5$  wt% NaCl), suggesting insignificant As transport by the vapor. At higher temperatures ( $400$  to  $700^\circ\text{C}$ ), however, As concentrations recently measured in vapor and brine inclusions in quartz from a variety of porphyry-style  $\text{Cu} \pm \text{Au} \pm \text{Mo} \pm \text{Sn}$  deposits (e.g., Grasberg, Bajo de la Alumbrera, Mole Granite, Zinnwald), reveal As enrichments in

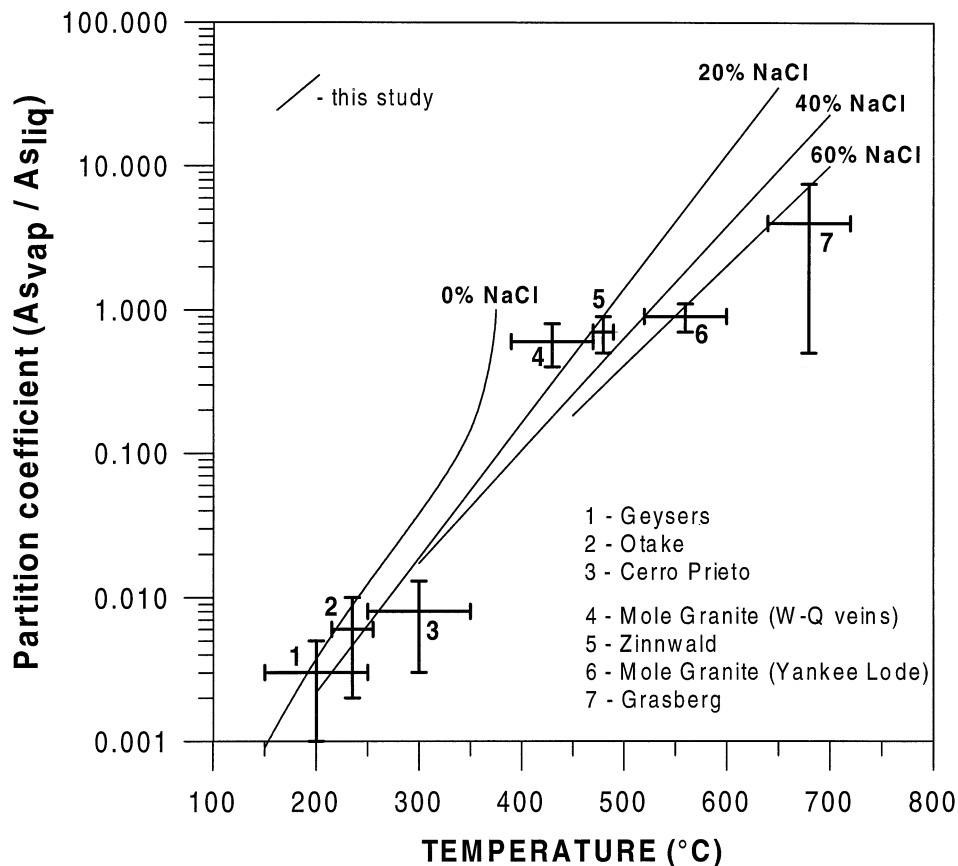


Fig. 14. Comparison between As vapor–liquid partitioning predicted in this study and observed in modern hydrothermal systems and fluid inclusions in quartz from magmatic–hydrothermal ore deposits. The error bars denote ranges of the As vapor–liquid partition coefficients and temperatures measured in active geothermal fields (1 to 3) and in ancient deposits (4 to 7) indicated by numbers in the figure and taken from the following references: 1, 2, and 3, Ballantyne and Moore (1988); 4 and 6, Audétat et al. (1998, Audétat et al., 2000) 5 and 7, Heinrich et al. (1999) and Ulrich et al. (1999). Solid lines = As vapor–liquid partition coefficients predicted in this study by using Eqn. 5 as a function of temperature at indicated NaCl content of the liquid.

the aqueous vapor phase in comparison to the coexisting NaCl-rich brine (30 to 60 wt% NaCl) (Audétat et al., 1998; Heinrich et al., 1999; Ulrich et al., 1999). Arsenic vapor-brine partition coefficients range from  $\sim 0.5$  to 10 at temperatures from 400 to 700°C, suggesting an important transport by the vapor phase produced via boiling of the ascending magmatic fluid (Heinrich et al., 1999).

In Figure 14 are also plotted  $\text{As}(\text{OH})_3$  partition coefficients measured in this study as a function of NaCl liquid-phase content and extrapolated to higher temperatures by Eqn. 5. It can be seen that the natural As vapor–liquid fractionations both for low-temperature dilute fluids and high-temperature vapor-brine systems are in good agreement with our predictions and can be interpreted by the formation of the  $\text{As}(\text{OH})_3$  species in the vapor phase through over the fluid evolution from magmatic to epithermal. Note that similar vapor–brine partition coefficients were also inferred for boron from the same fluid inclusions of magmatic-hydrothermal deposits (Audétat et al., 1998, Audétat et al., 2000). Boric acid,  $\text{B}(\text{OH})_3$ , is by far the most dominant species both in aqueous solution and high-temperature vapor (Styrikovich et al., 1960; Chase et al., 1985). The similarity of arsenic and boron vapor–liquid fractionation

patterns in hydrothermal environments is thus quantitatively explained by the close chemical speciation of both metalloids in the vapor and aqueous phases. The vapor-phase chemical speciation of copper and gold, which were found to partition more strongly than arsenic and boron, into the vapor phase in the same porphyry-style deposits (Heinrich et al., 1992; Ulrich et al., 1999), is probably different. Following the strong “chalcophile” character of both metals, it has been suggested that  $\text{Cu}(\text{I})$  and  $\text{Au}(\text{I})$  sulfide complexes may stabilize these metals in the  $\text{H}_2\text{S}$ -enriched vapor (Heinrich et al., 1992; Audétat et al., 1998). Experimental studies are, however, necessary to verify this hypothesis, as well as the possible formation of hydroxide or mixed OH-S complexes for Au and Cu in the vapor phase.

## 5.2. Volcanic Gases

Thermodynamic properties of the  $\text{As}(\text{III})$  hydroxide gaseous species derived in this study together with those available for other As gaseous complexes allow prediction of arsenic speciation in high-temperature volcanic gas emissions. Figure 15 shows an example of the equilibrium distribution of As species in a typical volcanic gas. Arsenic species abundances were

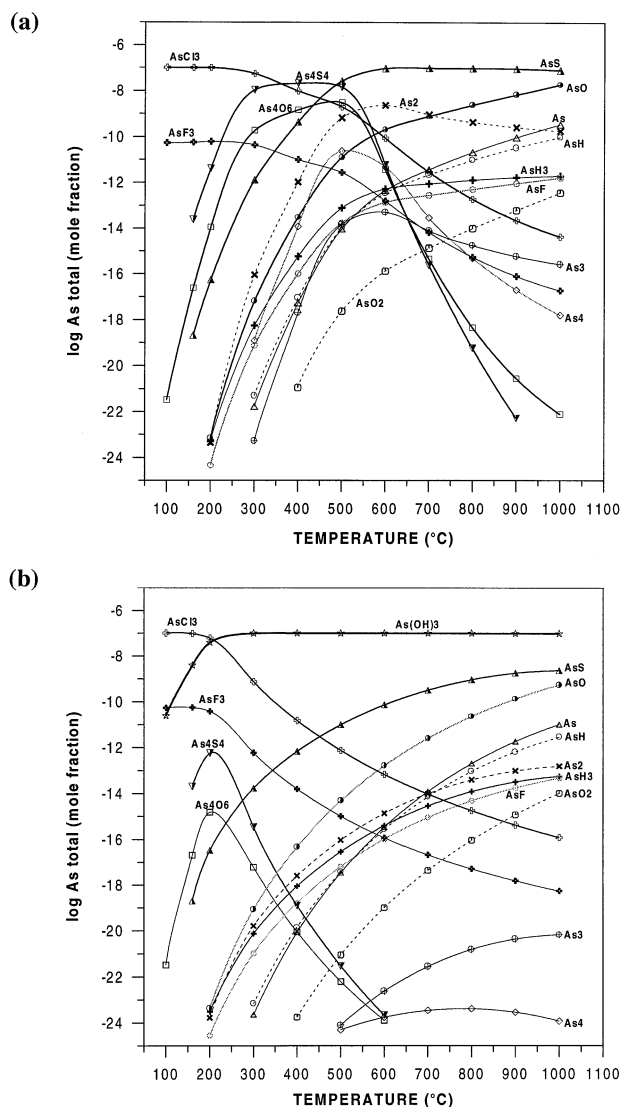


Fig. 15. Calculated distribution of As gaseous species (expressed in logarithm of As mole fraction in the gas) as a function of temperature at atmospheric pressure in a cooling magmatic gas from Kudryavy volcano, Kuril Islands. The following initial gas composition, typical of high-temperature fumarols of Kudryavy volcano, was adopted at 900°C (in mol%): H<sub>2</sub>O = 94.5, CO<sub>2</sub> = 2.0, H<sub>2</sub> = 1.0, SO<sub>2</sub> = 1.5, H<sub>2</sub>S = 0.5, HCl = 0.5, HF = 0.03, and As = 10<sup>-5</sup> (see text for details). Graph A corresponds to calculations using only anhydrous As species available in Gurvich et al. (1993). Graph B shows calculations in the presence of As(OH)<sub>3</sub>(gas) from this study. It can be seen that As(OH)<sub>3</sub>(gas) is by far the most dominant As species at temperatures above 200°C (see text for details).

calculated as a function of temperature at atmospheric pressure by using the GIBBS computer code (Shvarov and Bastrakov, 1999). The Gibbs free energies for gaseous species necessary to perform these calculations were generated by using the parameters reported in Table 4 for As(OH)<sub>3</sub> and As<sub>4</sub>O<sub>6</sub>; and taken from Robie et al. (1978) for H<sub>2</sub>O, CO<sub>2</sub>, CH<sub>4</sub>, CO, H<sub>2</sub>S, SO<sub>2</sub>, S<sub>2</sub>, H<sub>2</sub>, O<sub>2</sub>, HF, and HCl. The Gibbs free energies for elemental arsenic species (As, As<sub>2</sub>, As<sub>3</sub>, As<sub>4</sub>), hydrides (AsH, AsH<sub>3</sub>), sulfides (AsS, As<sub>4</sub>S<sub>4</sub>), oxides (AsO, AsO<sub>2</sub>), fluorides (AsF,

AsF<sub>3</sub>), and chloride (AsCl<sub>3</sub>) were taken from Gurvich et al. (1993). It should be noted that the thermodynamic properties of some of these anhydrous species can exhibit large uncertainties; and variations in free energies of several tens of kilojoules per mole exist for same species between different databases (e.g., Naumov et al., 1974; Pankratz, 1982; Symonds and Reed, 1993; Gurvich et al., 1993). In this study, we chose the most recent and complete database of Gurvich et al. (1993) for consistency. The initial gas composition was typical of that measured in high-temperature fumarols (800 to 950°C) of Kudryavy volcano, Iturup, Kuril Islands (Taran et al., 1995), and contained (in mol%), the following: H<sub>2</sub>O = 94.5, CO<sub>2</sub> = 2.0, H<sub>2</sub> = 1.0, SO<sub>2</sub> = 1.5, H<sub>2</sub>S = 0.5, HCl = 0.5, HF = 0.03, and As = 10<sup>-5</sup>. For simplicity, the redox state of the gas mixture was assumed to be controlled by equilibria between the gas components on cooling at all temperatures (Taran et al., 1995; Quisefit et al., 1989).

A first calculation was performed by using only anhydrous As species (Fig. 15a) and a second one including As(OH)<sub>3</sub> (Fig. 15b). It can be seen in Fig. 15a that AsCl<sub>3</sub>, As<sub>4</sub>S<sub>4</sub> + As<sub>4</sub>O<sub>6</sub>, and AsS + AsO dominate As gaseous speciation in the Kudryavy volcano gas at low (<300°C), moderate, and high temperatures (>700°C), respectively. The including As(OH)<sub>3</sub>(gas) in the calculations significantly change the species distribution. It can be seen in Figure 15b that As(OH)<sub>3</sub>(gas) largely dominates As speciation at temperatures above 300°C, accounting for more than 99% of the total As in the gas. Similar results (not shown) were also obtained for a different, more reducing, gas composition corresponding to that of Mt. St. Helens volcano, Alaska (Symonds and Reed, 1993). It should be noted that the Gibbs free energies of As(OH)<sub>3</sub> calculated above 600 to 800°C can exhibit variations of 30 to 40 kJ/mol corresponding to the uncertainties on the values of ΔG<sup>o</sup><sub>298</sub>, S<sup>o</sup>, and C<sub>p</sub><sup>o</sup>(T) derived in this study (Table 4). Nevertheless, even in such limits, As(OH)<sub>3</sub> still remains dominant. For example, at 700°C, if its Gibbs free energy were increased by 40 kJ/mol, As(OH)<sub>3</sub> would still account for more than 60% of total As in both Kudryavy and Mt. St. Helens gases. Thus, the results of this study show, for the first time, the important role of hydroxide species in As gaseous transport. This conclusion is also in agreement with the gaseous speciation of other chemically similar metals such as B, Mo, and W, which form similar hydroxide species (B(OH)<sub>3</sub>, H<sub>2</sub>MoO<sub>4</sub>, H<sub>2</sub>WO<sub>4</sub>) in hot volcanic vapors (Bernard et al., 1990; Churakov et al., 2000). In view of our results and these studies, it seems very likely that gas-phase hydrolysis and hydration play an important role in the speciation and transport of many metals and metalloids, especially those that exhibit a strong chemical affinity for OH groups in aqueous solution (e.g., Al, Fe, Sb, Si, REE, Zr, Re).

## 6. CONCLUDING REMARKS

Vapor-liquid and vapor-solid partitioning and XAFS spectroscopy measurements performed in this study demonstrate that the As(III) hydroxide complex As(OH)<sub>3</sub> is by far the most dominant As-bearing species in aqueous and vapor phase in the system H<sub>2</sub>O-NaCl ± HCl ± H<sub>2</sub>S, typical of natural hydrothermal environments, over a wide range of temperature (25 to 500°C) and fluid densities (1.1 to 0.05 g cm<sup>-3</sup>). Vapor-liquid partitioning for As both in pure water and NaCl-H<sub>2</sub>O fluids

above  $\sim 200^{\circ}\text{C}$  can be described as a simple function of vapor-to-liquid density ratio and temperature. The data obtained in this study allowed, for the first time, accurate prediction of As vapor-liquid distribution coefficients and generation of thermodynamic parameters for  $\text{As}(\text{OH})_3(\text{gas})$ .

Arsenic vapor-liquid fractionations observed both in modern geothermal fields and in fluid inclusions from magmatic-hydrothermal deposits are in good agreement with our measurements and can be quantitatively interpreted by the equilibrium  $\text{As}(\text{OH})_3(\text{aq}) = \text{As}(\text{OH})_3(\text{gas})$ . Moreover, thermodynamic calculations indicate that  $\text{As}(\text{OH})_3(\text{gas})$  is the dominant As-bearing species in high-temperature volcanic gases even at water pressures as low as 1 bar.

These results imply that hydroxide or hydrated species in the vapor phase could also be important for other major and trace elements exhibiting a high chemical affinity to OH groups in solution, such as Fe, Al, REE, Sb, Si, and Ge, for which currently available data are limited to anhydrous gaseous compounds. Explicit account for metal-water interactions in the vapor phase is thus necessary to accurately model metal behavior and transport during magma degassing and magmatic-to-hydrothermal fluid evolution.

*Acknowledgments*—This research was supported by French Ministère de l'Enseignement Supérieur et de la Recherche (awarding a grant "Coup de pouce for young scientist" to G.S.P.), CNRS/INSU ("Equipements mi-lourds"), and the Russian Foundation for Basic Research (grant 00-05-64266 to A.Yu.B.). We are grateful to the ESRF scientific committee (Grenoble, France) for providing beam time and access to the synchrotron facility. We thank Yvonne Soldo, Olivier Proux, Yoann Calzavara, and Jean-Jacques Menthonex for their generous help and professional assistance during XAFS measurements at BM 32 beamline of the ESRF. We thank Daniel Aberdam and Marcus Winterer for providing us with their programs for XAFS spectra treatment. François Farges is acknowledged for his help with spectra acquisition and modeling. We are indebted to Jean-Michel Bény for Raman spectroscopic analyses; and to Laurent Peilleron, Didier Bellenoue, André Lefevre, and Evgeny Sheimin for their help in constructing and setting up the experimental equipment. We are grateful to Anastasia Borisova for her courage in obtaining some inaccessible Russian articles and correcting an earlier version of the manuscript. Insightful discussions with Yury Alekhin, Alexey Yaroshevsky, Alexander Zotov, and Jacques Schott have been a source of motivation and inspiration during this long study. The constructive comments of the associate editor, Mike McKibben; reviewer Nikolai Akinfiyev; and two anonymous reviewers greatly improved the article's presentation.

*Associate editor:* M. A. McKibben

## REFERENCES

- Aberdam D. (1998) SEDEM, a software package for EXAFS extraction and modelling. *J. Synchrotron Rad.* **5**, 1287–1297.
- Akinfiyev N. N., Zotov A. V., and Nikonov A. P. (1992) Thermodynamic analysis of equilibria in the system  $\text{As}(\text{III})\text{-S}(\text{II})\text{-O-H}$ . *Geochem. Intl.* **29**(12), 109–121.
- Alekhin Yu. V. and Vakulenko A. G. (1988) Thermodynamic properties and solubility of  $\text{NaCl}$  in water vapour at  $300\text{--}500^{\circ}\text{C}$  up to 300 bar. *Geochem. Intl.* **25**(5), 97–110.
- Archibald S. M., Migdisov A. A., and Williams-Jones A. E. (2001) The stability of Au-chloride complexes in water vapor at elevated temperatures and pressures. *Geochim. Cosmochim. Acta* **65**, 4413–4423.
- Audétat A., Günther D., and Heinrich C. A. (1998) Formation of a magmatic-hydrothermal ore deposit: Insights with LA-ICP-MS analysis of fluid inclusions. *Science* **279**, 2091–2094.
- Audétat A., Günther D., and Heinrich C. A. (2000) Causes for large-scale metal zonation around mineralized plutons: Fluid inclusion LA-ICP-MS evidence from the Mole Granite, Australia. *Econ. Geol.* **95**, 1563–1581.
- Baes C. F. Jr. and Mesmer R. E. (1976) *The Hydrolysis of Cations*. Wiley.
- Ballantyne J. M. and Moore J. N. (1988) Arsenic geochemistry in geothermal systems. *Geochim. Cosmochim. Acta* **52**, 475–483.
- Ban V. S. and Knox B. E. (1970) Mass-spectrometric study of the laser-induced vaporization of compounds of arsenic and antimony with the elements of group VIa. *J. Chem. Phys.* **52**, 248–253.
- Beattie I. R., Livingston K. M. S., Ozin G. A., and Reynolds D. J. (1970) Single-crystal Raman spectra of arsenolite ( $\text{As}_4\text{O}_6$ ) and senarmontite ( $\text{Sb}_4\text{O}_6$ ): The gas-phase Raman spectra of  $\text{P}_4\text{O}_6$ ,  $\text{P}_4\text{O}_{10}$ , and  $\text{As}_4\text{O}_6$ . *J. Chem. Soc.*, A449–451.
- Behrens R. G. and Rosenblatt G. M. (1972) Vapor pressure and thermodynamics of octahedral arsenic trioxide (arsenolite). *J. Chem. Thermodynamics* **4**, 175–190.
- Belton G. R. and Jordan A. S. (1965) The volatilization of molybdenum in the presence of water vapor. *J. Phys. Chem.* **69**, 2065–2071.
- Bernard A., Symonds R. B., and Rose Jr. W. I. (1990) Volatile transport and deposition of Mo, W, and Re in high temperature magmatic fluids. *Appl. Geochem.* **5**, 317–326.
- Bischoff J. L. (1991) Densities of liquids and vapors in boiling  $\text{NaCl-H}_2\text{O}$  solutions: A PVTX summary from  $300$  to  $500^{\circ}\text{C}$ . *Am. J. Sci.* **291**, 309–338.
- Bischoff J. L., Rosenbauer R. J., and Pitzer K. S. (1986) The system  $\text{NaCl-H}_2\text{O}$ : Relations of vapor-liquid near the critical temperature of water and of vapor-liquid-halite from  $300$  to  $500^{\circ}\text{C}$ . *Geochim. Cosmochim. Acta* **50**, 1437–1444.
- Bischoff J. L. and Pitzer K. S. (1989) Liquid-vapor relations for the system  $\text{NaCl-H}_2\text{O}$ : Summary of the P-T-x surface from  $300$  to  $500^{\circ}\text{C}$ . *Am. J. Sci.* **289**, 217–248.
- Born Von M. (1920) Volumen und Hydratationswärme der Ionen. *Zeit. Physik.* **1**, 45–48.
- Bowers T. S. (1990) The deposition of gold and other metals: Pressure-induced fluid immiscibility and associated stable isotope signatures. *Geochim. Cosmochim. Acta* **55**, 2417–2434.
- Brimhall G. H. and Crerar D. A. (1987) Ore fluids: Magmatic to supergene. In *Thermodynamic Modeling of Geological Materials: Minerals, Fluids and Melts* (eds. I. S. E. Carmichael and H. P. Eugster), pp. 235–321. Reviews Miner 17, Mineralogical Society of America.
- Brumbach S. B. and Rosenblatt G. M. (1972) In-cavity laser Raman spectroscopy of vapors at elevated temperatures:  $\text{As}_4$  and  $\text{As}_4\text{O}_6$ . *J. Chem. Phys.* **56**, 3110–3117.
- Chang S. S. and Bestul A. B. (1971) Heat capacities of cubic, monoclinic, and vitreous arsenious oxide from  $5$  to  $350^{\circ}\text{K}$ . *J. Chem. Phys.* **55**, 933–946.
- Charlot G. (1966) *Les Méthodes de la Chimie Analytique: Analyse Quantitative Minérale*. Masson.
- Chase M. W. Jr., Davies C. A., Downey J. R. Jr., Frurip D. J., McDonald R. A., and Syverud A. N. (1985) JANAF thermochemical tables. 3rd ed. *J. Phys. Chem. Ref. Data* **14**(Suppl. 1) 1–1856.
- Churakov S. V., Tkachenko S. I., Korzhinskii M. A., Bocharnikov R. E., and Shmulovich K. I. (2000) Evolution of composition of high-temperature fumarolic gases from Kudryavy volcano, Iturup, Kuril Islands: The thermodynamic modeling. *Geochem. Intl.* **38**, 436–451.
- Collings M. D., Sherman D. M., and Ragnarsdottir V. K. (2000) Complexation of  $\text{Cu}^{2+}$  in oxidized  $\text{NaCl}$  brines from  $25$  to  $175^{\circ}\text{C}$ : Results from in situ EXAFS spectroscopy. *Chem. Geol.* **167**, 65–73.
- Dandurand J. -L. and Schott J. (1992) Prediction of ion association in mixed-crystal fluids. *J. Phys. Chem.* **96**, 7770–7777.
- Drummond S. E. and Ohmoto H. (1985) Chemical evolution and mineral deposition in boiling hydrothermal systems. *Econ. Geol.* **80**, 126–147.
- Ellis A. J. and Fyfe W. S. (1957) Hydrothermal chemistry. *Rev. Pure Appl. Chem.* **7**, 261–316.
- Farges F., Brown G. E. Jr., and Rehr J. J. (1996) Coordination chemistry of Ti(IV) in silicate glasses and melts: I. XAFS study of titanium coordination in oxide model compounds. *Geochim. Cosmochim. Acta* **60**, 3023–3038.
- Garrels R. M. and Christ C. L. (1965) *Solutions Minerals, and Equilibria*. Harper & Row.

- Goldschmidt V. M. (1954) *Geochemistry*. Oxford.
- Gout R., Pokrovski G. S., Schott J., and Zwick A. (1997) Raman spectroscopy study of arsenic speciation in aqueous solution to 275°C. *J. Raman Spect.* **28**, 725–730.
- Gurvich L. V., Iorish V. S., Belov G. B., Yungman V. S., and Veitz I. V. (1993) *IVTANTHERMO—A Thermodynamic Database and Software System for the Personal Computer*. CRC Press.
- Hashimoto A. (1992) The effect of H<sub>2</sub>O gas on volatilities of planet-forming major elements: I. Experimental determination of the thermodynamic properties of Ca-, Al-, and Si-hydroxide gas molecules and its application to the solar nebula. *Geochim. Cosmochim. Acta* **56**, 511–532.
- Hedenquist J. W. and Lowenstern J. B. (1994) The role of magmas in the formation of hydrothermal ore deposits. *Nature* **370**, 519–527.
- Heinrich C. A. and Eadington P. J. (1986) Thermodynamic predictions of the hydrothermal chemistry of arsenic and their significance for the paragenetic sequence of some cassiterite–arsenopyrite–base metal sulfide deposits. *Econ. Geol.* **81**, 511–529.
- Heinrich C. A., Ryan C. G., and Ternagh P. M. (1992) Segregation of ore metals between brine and vapor: A fluid inclusion study using PIXE microanalysis. *Econ. Geol.* **87**, 1566–1583.
- Heinrich C. A., Günther D., Audétat A., Ulrich T., and Frischknecht R. (1999) Metal fractionation between magmatic brine and vapour, and the link between porphyry-style and epithermal Cu-Au deposits. *Geology* **27**, 755–758.
- Helz G. R., Tossel J. A., Charnock J. M., Patrick R. A. D., Vaughan D. J., and Garner C. D. (1995) Oligomerization in As(III) sulfide solutions: Theoretical and spectroscopic evidence. *Geochim. Cosmochim. Acta* **59**, 4591–4604.
- Hoffmann M. M., Darab J. G., Heald S. M., Yonker C. R., and Fulton J. L. (2000) New experimental developments for in situ XAFS studies of the chemical reactions under hydrothermal conditions. *Chem. Geol.* **167**, 89–103.
- Jungermann E. and Plieth K. (1967) Dampfdrucke und Kondensationsgeschwindigkeiten der polymorphen Arsen- und Antimontrioxide. *Zeit. Phys. Chem.* **53**, 215–228.
- Karutz I. and Stranski I. N. (1957) Über die Verdampfung von Arsenolith und Claudetit. *Zeit. Anorg. Allgem. Chem.* **292**, 330–342.
- Kazenas E. K. and Tsvetkov J. N. (1997) *Evaporation of Oxides*. Nauka (in Russian).
- Kestin J., Sengers J. V., Kamgar-Parsi B., and Levelt Sengers J. M. H. (1984) Thermophysical properties of fluid H<sub>2</sub>O. *J. Phys. Chem. Ref. Data* **13**, 175–183.
- Khaibullin I. K. and Borisov N. M. (1966) Experimental investigation of the thermal properties of aqueous and vapor solutions of sodium and potassium chlorides at phase equilibrium. *Teplotfizika Vysokih Temperatur.* **4**, 518–523 (in Russian).
- Lewis G. N. and Randall M. (1965) *Thermodynamics*. 2nd ed. International Student Edition. Mexico.
- Loehr T. M. and Plane R. A. (1968) Raman spectra and structure of arsenious acid and arsenite in aqueous solution. *J. Inorg. Chem.* **7**, 1708–1714.
- Maier C. G. and Kelley K. K. (1932) An equation for the representation of high-temperature heat content data. *J. Am. Chem. Soc.* **54**, 3243–3246.
- Mambo V. S., Yoshida M., and Matsuo S. (1991) Partition of arsenic and phosphorus between volcanic gases and rock. Part I: Analytical data and magmatic conditions of Mt. Usu, Japan. *J. Volcanol. Geotherm. Res.* **46**, 37–47.
- Marczenko Z. (1986) *Separation and Spectrophotometric Determination of Elements*. Ellis Horwood.
- Martynova O. I. (1964) Some questions on the solubility of low-volatile inorganic compounds in water steam at high temperatures and pressures. *Zh. Fiz. Khim.* **38**, 1065–1076 (in Russian).
- Mayanovic R. A., Anderson A. J., Bassett W. A., and Chou I. M. (2001) Hydrogen bond breaking in aqueous solutions near the critical point. *Chem. Phys. Lett.* **336**, 212–218.
- Migdisov A. A. and Bychkov A. Yu. (1998) The behavior of metals and sulfur during the formation of hydrothermal mercury-antimony-arsenic mineralization, Uzon caldera, Kamchatka, Russia. *J. Volcanol. Geotherm. Res.* **84**, 153–171.
- Migdisov A. A., Suleimenov O. M., and Alekhin Y. V. (1998) Experimental study of polysulfane stability in gaseous hydrogen sulfide. *Geochim. Cosmochim. Acta* **62**, 2627–2635.
- Migdisov A. A., Williams-Jones A. E., and Suleimenov O. M. (1999) Solubility of chlorargyrite (AgCl) in water vapor at elevated temperatures and pressures. *Geochim. Cosmochim. Acta* **63**, 3817–3827.
- Mosselmans J. F. W., Schofield P. F., Charnock J. M., Garner C. D., Patrick R. A. D., and Vaughan D. J. (1996) X-ray absorption studies of metal complexes in aqueous solution at elevated temperatures. *Chem. Geol.* **127**, 339–350.
- Naumov G. B., Ryzhenko B. N., and Khodakovskiy I. L. (1974) *Handbook of Thermodynamic Data*. U.S. Geological Survey.
- Oelkers E. H., Sherman D. M., Ragnarstottir K. V., and Collins C. (1998) An EXAFS spectroscopic study of aqueous antimony(III)-chloride complexation at temperatures from 25 to 250°C. *Chem. Geol.* **151**, 21–27.
- Pankratz L. B. (1982) Thermodynamic properties of elements and oxides. *Bur. Min. Bull.* **672**.
- Pauling L. (1948) *The Nature of the Chemical Bond*. Cornell University Press.
- Pertlik F. (1978) Structure refinement of cubic As<sub>2</sub>O<sub>3</sub> (arsenolite) with single-crystal data. *Czech. J. Phys.* **B28**, 170–176 (in German).
- Pitzer K. S. and Pabalan R. T. (1986) Thermodynamics of NaCl in steam. *Geochim. Cosmochim. Acta* **50**, 1445–1454.
- Pokrovski G. S. (1996) Experimental study of the behavior of germanium, silicon and arsenic, and of aluminum-silica complexing in natural solutions. Ph.D. thesis, Paul-Sabatier University, Toulouse (in French).
- Pokrovski G. S., Gout R., Zotov A., Schott J., and Harrichoury J.-C. (1996) Thermodynamic properties and stoichiometry of the arsenic(III) hydroxide complexes at hydrothermal conditions. *Geochim. Cosmochim. Acta* **60**, 737–749.
- Pokrovski G. S., Bény J.-M., and Zotov A. V. (1999) Solubility and Raman spectroscopic study of As(III) speciation in organic compound–water solutions: A hydration approach for aqueous arsenic in complex solutions. *J. Soln. Chem.* **28**, 1307–1327.
- Pokrovski G. S., Martin F., Hazemann J.-L., and Schott J. (2000) An X-ray absorption fine structure spectroscopy study of germanium–organic ligand complexes in aqueous solution. *Chem. Geol.* **163**, 151–165.
- Pokrovski G. S., Kara S., and Roux J. (2002a) Stability and solubility of arsenopyrite, FeAsS, in crustal fluids. *Geochim. Cosmochim. Acta* **66**, 2361–2378.
- Pokrovski G. S., Schott J., Hazemann J.-L., Farges F., and Pokrovskiy O. S. (2002b) An X-ray absorption fine structure (XAFS) and nuclear magnetic resonance (NMR) spectroscopy study of gallium–silica complexes in aqueous solution. *Geochim. Cosmochim. Acta* in press.
- Potter R. W. and Brown D. L. (1977) *The Volumetric Properties of Aqueous Sodium Chloride Solutions from 0° to 500°C at Pressures up to 2000 bars Based on a Regression of Available Data in the Literature*. U.S. Geological Survey Bulletin 1421-C.
- Press W. H., Flannery B. P., Teukolsky S. A., and Vetterling W. T. (1986) *Numerical Recipes—The Art of Scientific Computing*. Cambridge University Press.
- Quisefit J. P., Toutain J. P., Bergametti G., Javoy M., Cheynet B., and Person A. (1989) Evolution versus cooling of gaseous volcanic emissions from Momotombo Volcano, Nicaragua: Thermochemical model and observations. *Geochim. Cosmochim. Acta* **53**, 2591–2608.
- Robie R. A., Hemingway B. S., and Fisher J. R. (1978) Thermodynamic properties of minerals and related substances at 298.15 K and 1 bar (10<sup>5</sup> pascals) pressure and at higher temperatures. *Bull. Geol. Surv.* **1452**, 1–456.
- Rushton E. R. and Daniels F. (1926) The vapor pressure of arsenic trioxide. *J. Am. Chem. Soc.* **48**, 384–389.
- Sandler S. I. (1985) *Chemical and Engineering Thermodynamics*. 3rd ed. Wiley.
- Schulman J. H. and Schumb W. C. (1943) The polymorphism of arsenious oxide. *J. Am. Chem. Soc.* **65**, 878–883.
- Sergeeva E. I. and Khodakovskiy I. L. (1969) Physical chemical condition of native arsenic formation in hydrothermal deposits. *Geokhimiya* **7**, 846–858 (in Russian).

- Setchénow M. (1892) Action de l'acide carbonique sur les solutions à acides forts. *Ann. Chim. Phys.* **25**, 225–270.
- Seward T. M., Henderson C. M. B., Charnock J. M., and Dobson B. R. (1996) An X-ray absorption (EXAFS) spectroscopic study of aequated Ag in hydrothermal solutions to 350°C. *Geochim. Cosmochim. Acta* **60**, 2273–2282.
- Seward T. M., Henderson C. M. B., Charnock J. M., and Driesner T. (1999) An EXAFS study of solvation and ion pairing in aqueous strontium solutions to 300°C. *Geochim. Cosmochim. Acta* **63**, 2409–2418.
- Shock E. L., Oelkers E. H., Johnson J. W., Sverjensky D. A., and Helgeson H. C. (1992) Calculation of the thermodynamic properties of aqueous species at high pressures and temperatures: Effective ionic radii, dissociation constants, and standard partial molal properties to 1000°C and 5 kbar. *J. Chem. Soc. Faraday Trans.* **88**, 803–826.
- Shock E. L., Sassani D. C., Willis M., and Sverjensky D. A. (1997) Inorganic species in geological fluids: Correlations among standard molal thermodynamic properties of aqueous ions and hydroxide complexes. *Geochim. Cosmochim. Acta* **61**, 907–950.
- Shvarov Yu. V. and Bastrakov E. N. (1999) *HCh: A Software Package for Geochemical Equilibrium Modeling*. Record 1999/25. Australian Geological Survey Organization.
- Simonson J. M. and Palmer D. A. (1993) Liquid-vapor partitioning of HCl(aq) to 350°C. *Geochim. Cosmochim. Acta* **57**, 1–7.
- Smith R. W., Popp C. J., and Norman D. I. (1986) The dissociation of oxy-acids at elevated temperatures. *Geochim. Cosmochim. Acta* **50**, 137–142.
- Smith C. L., Fickin W. H., and Thompson J. M. (1987) Concentrations of arsenic, antimony, and boron in steam and steam condensate at the Geysers, California. *J. Volcanol. Geothermal. Res.* **32**, 329–341.
- Soldo Y., Hazemann J.L., Aberdam D., Inui M., Tamura K., Raoux D., Pernot E., Jal J. F., and Dupuy-Philon J. (1998) Semiconductor-to-metal transition in fluid selenium at high pressure and temperature: An investigation using X-ray absorption spectroscopy. *Phys. Rev. B* **57**, 258–268.
- Styrikovich M. A., Khaibullin I. K., and Tshvirashvili D. G. (1955) A study of salt solubility in high-pressure water steam. *Doklady AN SSSR* **100**, 1123–1126 (in Russian).
- Styrikovich M. A., Martynova O. I., Khaibullin I. K., and Mingulina E. I. (1959) Some features of the transfer of weak inorganic acids into the saturated vapor. *Teploenergetika* **9**, 50–56 (in Russian).
- Styrikovich M. A., Tshvirashvili D. G., and Heberidze D. P. (1960) A study of the solubility of boric acid in saturated water vapor. *Doklady AN SSSR* **134**, 615–617 (in Russian).
- Suleimenov O. M. and Krupp R. E. (1994) Solubility of hydrogen sulfide in pure water and NaCl solutions, from 20 to 320°C and at saturation pressures. *Geochim. Cosmochim. Acta* **58**, 2433–2444.
- Symonds R. B. (1990) Applications of multicomponent chemical equilibria to volcanic gases at Augustine Volcano, volcanic halogen emissions, and volcanological studies of gas-phase transport. Ph.D. thesis. Michigan Technological University.
- Symonds R. B., Rose W. I., Reed M. H., Lichte F. E., and Finnegan D. L. (1987) Volatilization transport and sublimation of metallic and non-metallic elements in high-temperature gases at Merapi Volcano, Indonesia. *Geochim. Cosmochim. Acta* **51**, 2083–2101.
- Symonds R. B. and Reed M. H. (1993) Calculation of multicomponent chemical equilibria in gas–solid–liquid systems: Calculation methods, thermochemical data, and applications to studies of high-temperature volcanic gases with examples from Mount St. Helens. *Am. J. Sci.* **293**, 758–864.
- Sweeton F. H., Mesmer R. E., and Baes C. F. Jr. (1974) Acidity measurements at elevated temperatures. VII. Dissociation of water. *J. Soln. Chem.* **3**, 191–214.
- Tagirov B. R., Zotov A. V., and Akiniev N. N. (1997) Experimental study of the dissociation of HCl from 350 to 500°C and from 500 to 2500 bar. Thermodynamic properties of HCl<sup>0</sup>(aq). *Geochim. Cosmochim. Acta* **61**, 4267–4280.
- Tamura K., Inui M., and Hosokawa S. (1995) XAFS measurements at high temperatures and pressures. *Rev. Sci. Instrum.* **66**, 1382–1384.
- Taran Yu. A., Hedenquist J. W., Korzhinsky M. A., Tkachenko S. I., and Shmulovich K. I. (1995) Geochemistry of magmatic gases from Kudryavy volcano, Iturup, Kuril Islands. *Geochim. Cosmochim. Acta* **59**, 1749–1761.
- Teo B. K. (1986). *EXAFS: Basic Principles and Data Analysis: Inorganic Chemistry Concepts*. Vol. 9, Springer-Verlag.
- Tossell J. A. (1997) Theoretical studies on arsenic oxide and hydroxide species in minerals and in aqueous solution. *Geochim. Cosmochim. Acta* **61**, 1613–1623.
- Ulrich T., Günther D., and Heinrich C. A. (1999) Gold concentrations of magmatic brines and the metal budget of porphyry copper deposits. *Nature* **399**, 676–679.
- Walther J. V. (1997) Determination of activity coefficients of neutral species in supercritical H<sub>2</sub>O solutions. *Geochim. Cosmochim. Acta* **61**, 3311–3318.
- Walther J. V. and Schott J. (1988) The dielectric constant approach to speciation and ion pairing at high temperature and pressure. *Nature* **332**, 635–638.
- Winterer M. (1997) The XAFS-a data analysis program for material sciences. In Proceedings of the 9th International Conference on X-ray Absorption Fine Structure (XAFS-IX), Grenoble, 1996 (eds. J. Goulon, C. Goulon-Ginet, N. B. Brookes), *J. Physique IV*, vol. 7; p. C2–243.
- Zabinsky S. Y., Rehr J. J., Ankudinov A. L., Albers R. S., and Eller M. J. (1995) Multiple scattering calculations of X-ray absorption spectra. *Phys. Rev. B* **52**, 2995–3009.
- Zakaznova-Iakovleva V. P., Migdisov A. A., Suleimenov O. M., Williams-Jones A. E., and Alekhin Y. V. (2001) An experimental study of stibnite solubility in gaseous hydrogen sulfide from 200 to 320°C. *Geochim. Cosmochim. Acta* **65**, 289–298.
- Zakirov I. V. and Sretenskaya N. G. (1994) A method of experimental determination of phase compositions at heterogeneous conditions. In *Experimental Problems of Geology*, pp. 664–667. Nauka (in Russian).

## APPENDIX

Table A1. Arsenic (III) concentrations in aqueous solution of arsenious acid ( $\text{As}_2\text{O}_3$  + pure water  $\pm$  0.1m NaCl) and its saturated vapor, and corresponding As(III) vapor/liquid partition coefficients at 250, 300, and 350°C and  $P_{\text{sat}}$ .

Run	P (bar)	Duration (d)	$m_{\text{As}}$ liquid (mol/kg solution)	$m_{\text{As}}$ vapor (mol/kg vapor)	$K_m$ (As) (vapor/liquid)	Sampling procedure <sup>a</sup>
250°C ( $\text{H}_2\text{O} \pm 0.1\text{m NaCl}$ )						
Y	39.0	1	0.0993	0.00081	0.008	ext
AG	39.2	4	0.158	0.0014	0.009	amp
AM	38.4	10	0.454	0.0058	0.013	amp
AC	38.3	2	0.519	0.0068	0.013	amp
AD	38.2	2	0.537	0.0076	0.014	amp
AJ	39.0	6	0.781	0.0093	0.012	amp
AL	37.9	11	1.02	0.014	0.014	amp
AO	36.3	21	2.96	0.049	$K_{\text{mean}} = 0.012 \pm 0.003$ 0.017	amp
300°C ( $\text{H}_2\text{O}$ )						
A1	85.0	0.7	0.104	0.0022	0.021	ext
A2	84.5	1.8	0.124	0.010	0.080	ext
A3	85.0	2.8	0.172	0.013	0.073	ext
A4	— <sup>b</sup>	3.8	0.20	0.018	0.091	ext
A5	—	4.7	0.32	0.012	0.036	ext
A6a	81.3	5.5	0.53	0.040	0.075	amp
A6b	81.1	5.6	0.63	0.019	0.031	ext
B1	86.2	1	0.032	0.0020	0.063	ext
B2	86.1	4	0.037	0.0014	0.038	ext
B3	85.5	6	0.041	0.0023	0.056	ext
B4a	84.0	9	0.045	0.0028	0.062	ext
B4b	83.0	9	0.052	0.0031	0.060	amp
C1	—	2	0.053	0.0017	0.033	ext
C2	—	4	0.058	0.0038	0.066	ext
C3	85.7	6	0.064	0.0056	0.087	ext
C4	86.2	12	0.073	0.0049	0.067	ext
C5a	84.5	13	0.084	0.0064	0.076	amp
C5b	84.5	13	0.084	0.075	0.090	ext
$K_{\text{mean}} = 0.063 \pm 0.023$						
350°C ( $\text{H}_2\text{O} \pm 0.1\text{m NaCl}$ )						
AF1	165.6	1	0.0024	0.00044	0.183	ext
AF1	165.2	2	0.0031	0.00045	0.145	ext
AF3	165.0	3	0.0047	0.00062	0.132	ext
AD1	165.5	5	0.011	0.0018	0.164	ext
AD2	165.0	6	0.013	0.0020	0.154	ext
AJ1	166.3	1	0.028	0.0042	0.150	ext
AJ2	165.5	3	0.038	0.0050	0.132	ext
AC1	165.6	2	0.121	0.018	0.149	ext
AC2	165.0	4	0.147	0.021	0.143	ext
AC3	164.4	6	0.182	0.023	0.126	ext
$K_{\text{mean}} = 0.145 \pm 0.02$						
U	163.5	2	0.42	0.053	0.133	amp
AE1	163.1	1	0.62	0.081	0.130	ext
AE2	161.3	2	0.71	0.081	0.114	ext
AE3	160.2	5	0.84	0.093	0.111	ext
AL1	158.4	2	1.80	0.16	0.089	ext
AL2	154.4	3	2.10	0.19	0.090	ext
AL3	152.2	4	2.46	0.21	0.085	ext

<sup>a</sup> ext indicates vapor was extracted through a capillary tubing ("extraction technique"; see text); amp indicates vapor was trapped in situ in a Ti ampoule ("ampoule technique"; see text).

<sup>b</sup> Pressure was not measured in these runs.

Table A2. Arsenic (III), HCl, and H<sub>2</sub>S concentrations in aqueous solution and its saturated vapor and corresponding As(III) vapor/liquid partition coefficients at 350°C and P<sub>sat</sub>.

Run	P (bar)	Duration (d)	m <sub>HCl or H<sub>2</sub>S</sub> liquid (mol/kg)	m <sub>As</sub> liquid (mol/kg)	m <sub>As</sub> vapor (mol/kg)	m <sub>HCl or H<sub>2</sub>S</sub> vapor (mol/kg)	K <sub>m</sub> (As) vapor/liquid	Sampling procedure
H <sub>2</sub> O-HCl								
AU1	165.9	1	0.00067	0.0088	0.0014	0.00033	0.159	ext
AU2a	166.0	3.0	0.00074	0.0105	0.0021	0.00037	0.200	ext
AU2b	166.5	3.2	0.00082	0.0130	0.0023	0.00041	0.177	amp
AH1	165.9	1	0.0096	0.032	0.0050	0.0110	0.157	ext
AH2	165.4	4	0.0098	0.035	0.0055	0.0104	0.157	ext
AG1	168.0	1	0.088	0.036	0.0059	0.155	0.164	ext
AG2	168.0	2	0.079	0.043	0.0070	0.130	0.163	ext
AG3	166.0	4	0.076	0.050	0.0083	0.112	0.166	ext
							K <sub>mean</sub> = 0.165 ± 0.015	
H <sub>2</sub> O-H <sub>2</sub> S (+ 0.001m HCl)								
AS1	168.3	1	0.058	0.0088	0.0010	0.16	0.114	ext
AS2a	168.0	2	0.046	0.0104	0.0022	0.13	0.212	ext
AS2b	168.0	2.3	0.044	0.0123	0.0023	0.097	0.187	amp
AT1	168.2	1	0.19	0.0089	0.0014	0.55	0.157	ext
AT2	166.5	2	0.14	0.0110	0.0013	0.43	0.118	ext
AT3a	165.3	3	0.12	0.0134	0.0017	0.34	0.127	ext
AT3b	165.3	3.2	0.10	0.0160	0.0018	0.30	0.113	amp
							K <sub>mean</sub> = 0.146 ± 0.037	

Table A3. Arsenious acid concentrations in NaOH-H<sub>2</sub>O aqueous solution and its saturated vapor, and corresponding As(III) vapor/liquid partition coefficients as a function of pH at 350°C, P<sub>sat</sub>.

Run	P (bar)	Duration (d)	m <sub>NaOH</sub> liquid (mol/kg)	pH <sub>calc</sub> <sup>350°</sup> liquid <sup>a</sup>	m <sub>As</sub> liquid (mol/kg)	m <sub>As</sub> vapor (mol/kg)	K (As) vapor/liquid	Sampling procedure
AR1	165.7	2	0.00628	8.47	0.0375	0.0056	0.150	ext
AR2	163.0	6	0.00843	8.44	0.0450	0.0085	0.189	ext
AO1	—	2	0.0263	9.27	0.0385	0.0029	0.075	ext
AO2	—	3	0.0326	9.29	0.0468	0.0035	0.075	ext
AP1	164.6	1	0.0480	9.89	0.0360	0.00094	0.026	ext
AP2	163.7	2	0.0574	9.93	0.0420	0.0012	0.029	ext

<sup>a</sup> Solution pH was calculated from NaOH and As(OH)<sub>3</sub> aqueous concentration and using the dissociation constants of H<sub>2</sub>O, NaOH, and As(OH)<sub>3</sub> at 350°C and P<sub>sat</sub> according to Sweeton et al. (1974), Shock et al. (1997), and Pokrovski (1996), respectively.

Table A4. Arsenic (III) and NaCl concentrations in aqueous sodium chloride–arsenious acid solutions and their saturated vapor, and corresponding As(III) and NaCl vapor/liquid partition coefficients at 300, 350, 400, and 450°C.

Run	P (bar)	Duration (d)	$m_{\text{NaCl}}$ liquid mol/kg solution	$m_{\text{As}}$ liquid mol/kg solution	$m_{\text{As}}$ vapor mol/kg vapor	$K_m$ As vapor/liquid	$m_{\text{NaCl}}$ vapor mol/kg vapor	$K_m$ NaCl vapor/liquid	Sampling procedure
300°C									
D1	79.2	3	1.85	0.0530	0.00118	0.022	— <sup>a</sup>	—	ext
D2	78.0	5	1.95	0.0566	0.00141	0.025	—	—	ext
D3	76.2	7	2.21	0.0638	0.00151	0.024	—	—	ext
D4	72.0	9	2.71	0.0778	0.00167	0.021	—	—	ext
D5	68.4	11	3.67	0.105	0.0023	0.022	$7.4 \times 10^{-5}$	$2.0 \times 10^{-5}$	ext
D6	59.2	14	4.96	0.140	0.0030	0.021	$7.8 \times 10^{-5}$	$1.6 \times 10^{-5}$	ext
350°C									
AB1	159.0	1	1.21	0.125	0.010	0.080	0.00047	0.00039	ext
AB2	154.8	2	1.49	0.150 <sup>b</sup>	0.0076	0.051	0.00024	0.00016	ext
AB3	151.0	6	1.79	0.176 <sup>b</sup>	0.0050	0.028	0.00016	0.00009	ext
AB4	148.2	7	2.33	0.230 <sup>b</sup>	0.0038	0.017	—	—	ext
AK1	139.2	1	3.50	0.0317	0.0018	0.057	0.00036	0.00010	ext
AK2	133.7	3	4.08	0.0376	0.00133	0.035	0.00006	0.00002	ext
AK3	126.4	4	4.71	0.0422	0.00133	0.032	0.00043	0.00009	ext
400°C									
A1	234	1	4.18	0.039	0.0059	0.151	0.00048	0.00011	ext
A2	221	2	4.95	0.044	0.0059	0.034	0.00014	0.00003	ext
A3a	200	3	6.08	0.053	0.0064	0.121	0.00013	0.00002	ext
A3b	173	3.2	7.82	0.070	0.0056	0.080	0.00540	0.00069	amp
B1	267	0.3	1.80	0.056	0.013	0.232	0.0170	0.00944	ext
B2	246	1	3.43	0.074	0.015	0.203	0.0056	0.00163	ext
B3	222	2	4.84	0.125	0.015	0.120	0.00016	0.00003	ext
B4a	192	2.8	6.90	0.135	0.023	0.170	0.0120	0.00174	amp
B4b	189	3	7.03	0.150	0.016	0.107	0.00012	0.00002	ext
450°C									
A1	356	0.4	5.30	0.035	0.011	0.314	0.033	0.00623	ext
A2	321	1.0	6.66	0.040	0.011	0.275	0.015	0.00225	ext
A3	286	1.4	7.84	0.046	0.011	0.239	0.005	0.00064	ext
A4a	247	2.0	8.98 <sup>c</sup>	0.057	0.014	0.246	0.077	0.00857	amp
A4b	247	2.1	8.98 <sup>c</sup>	0.057	0.014	0.230	0.004	0.00045	ext

<sup>a</sup> Not determined.<sup>b</sup> Partial oxidation of As<sup>(III)</sup> to As<sup>(V)</sup> was detected in the liquid phase but could not be quantified (these data points were not taken into account).<sup>c</sup> Solution saturated with respect to solid NaCl.Table A5. Arsenic (V) concentrations in aqueous solution of arsenic acid (As<sub>2</sub>O<sub>5</sub> + pure water) and its saturated vapor, and corresponding As(V) vapor/liquid partition coefficients at 350°C and P<sub>sat</sub>.

Run	P (bar)	Duration (d)	$m_{\text{As(V)}}$ liquid (mol/kg)	$m_{\text{As(V)}}$ vapor (mol/kg)	$K_m$ (As) vapor/liquid	Sampling procedure
AF1	165.6	1	0.0067	0.00030	0.045	ext
AF1	165.2	2	0.0089	0.00032	0.036	ext
AF3	165.0	3	0.0133	0.00043	0.032	ext
AD1	165.5	5	0.024	0.0011	0.046	ext
AD2	165.0	6	0.029	0.0013	0.045	ext
AN1	165.0	1	0.040	0.0016	0.040	ext
AN2	165.0	2	0.048	0.0015	0.032	ext
$K_{\text{mean}} = 0.039 \pm 0.006$						

Table A6. Solubility of crystalline (250°C) and molten (350°C) As<sub>2</sub>O<sub>3</sub> in water vapor measured using the ampoule technique.

Run	Pressure measured (bar)	Duration (d)	Mass of As in ampoule <sup>a</sup> (mg)	Mass of H <sub>2</sub> O in ampoule (mg)	C <sub>As</sub> vapor (mol cm <sup>-3</sup> ) (×10 <sup>7</sup> )
250°C					
E	0	2.5	0.95	0	13.76
G	0	7	1.00	10	14.48
J	0	4	0.36	0	5.213
AS	0	7	0.61	0	8.833
H	10.7	2.5	0.61	42.2	8.833
I	11.3	10.5	0.53	45.3	7.674
A <sup>b</sup>	30.6	1.5	0.13	129.0	1.882
F	31.1	8	0.61	135.2	8.833
B	31.7	3.5	0.52	135.3	7.529
D	32.1	2.5	0.39	134.4	5.647
C	32.5	12.5	0.53	142.3	7.674
K	37.0	9.5	0.57	187.2	8.253
L sat <sup>c</sup>	37.0	3.5	1.02	180.7	14.77
AP	34.8	7	0.41	143.3	5.937
AQ sat	36.0	7	0.52	145.0	7.529
AR sat	37.0	7	0.50	151.3	7.240
AT sat	36.5	15	0.59	147.0	8.543
350°C					
D	0	3	6.4	0	92.67
L	0	17	9.2	0	121.1
T	6.0	13	5.6	29.2	81.09
F	10.0	9	6.7	25.2	97.01
AV	16.6	4	5.1	34.6	73.85
AX	46.6	4	7.4	143.6	107.2
G	67.6	6	8.3	220.0	120.2
AY	77.5	5	8.5	283.2	123.1
B	95.0	3	8.3	424.0	120.2
H	105.3	5	10.8	395.7	156.4
N	115.1	2	12.3	468.8	178.1
AI <sup>d</sup>	117.5	2	—	—	78.00
M	123.1	3	12.5	528.5	181.0
E	143.0	13	13.4	700.3	194.0
C	150.0	3	12.4	797.6	179.6

<sup>a</sup> Ampoule volume = 9.22 ± 0.05 cm<sup>3</sup>.

<sup>b</sup> Equilibrium is likely to be not attained in this run.

<sup>c</sup> sat indicates presence of an aqueous solution saturated with respect to As<sub>2</sub>O<sub>3</sub>.

<sup>d</sup> Sampling through capillary tubing produced lower As concentrations (not taken into account).

Table A7. Solubility of crystalline  $\text{As}_2\text{O}_3$  in undersaturated water vapor at 130, 220, 265, and 300°C measured via the quenching technique.

Run	$P_{\text{H}_2\text{O}}^{\text{a}}$ (bar)	Duration (d)	$C_{\text{As vapor}}^{\text{b}}$ ( $\text{mol cm}^{-3}$ ) ( $\times 10^7$ )
130°C			
20	0	15	0.0142
19	0	15	0.0085
18	0.4	15	0.0077
17	0.9	15	0.0083
16	1.3	15	0.0098
15	1.8	15	0.0103
14	2.2	15	0.0069
13	2.3	15	0.0067
220°C			
20	0.7	10	1.78
4c	5.0	10	2.25
3c	9.5	10	2.87
2c	19.2	10	2.99
265°C			
20	0	10	34.57
19	0.3	10	22.00
18	0.3	10	26.67
17	1.2	10	22.44
16	1.2	10	23.00
15	2.9	10	16.90
14	39.5	10	16.79
13	39.7	10	18.50
300°C			
2c	0	10	52.34
1c	0	10	62.92
20	6.5	10	100.2
19	6.8	10	100.5
3c	26.9	10	97.56
4c	27.3	10	99.78
14	30.5	10	98.00
9	54.3	10	102.4
2	73.9	10	88.78
6	75.2	10	90.00

<sup>a</sup>  $P_{\text{H}_2\text{O}}$  was calculated from the mass of water loaded in the reactor and the reactor-free volume, and using the PVT properties of pure water (Kestin et al. 1984).

<sup>b</sup> Determined from  $\text{As}_2\text{O}_3$  quantity condensed on the reactor walls after quenching (see text for details).